

Late Paleocene – Middle Eocene magmatic flare-up in western Anatolia

Aral I. Okay^{a,*}, Gültekin Topuz^a, Andrew R.C. Kylander-Clark^b, Sarah Sherlock^c,
Massimiliano Zattin^d

^a Eurasia Institute of Earth Sciences, İstanbul Technical University, 34469 Maslak, İstanbul, Turkey

^b Department of Earth Sciences, University of California, Santa Barbara, CA, USA

^c School of Physical Sciences, STEM Faculty, The Open University, Milton Keynes, UK

^d Department of Geosciences, University of Padua, Padua, Italy

ARTICLE INFO

Keywords:

Paleocene-Eocene magmatism
Magmatic flare-up
Geochronology
Western Anatolia
Slab break-off
Post-collision
Subduction

ABSTRACT

A 3000-km long magmatic belt of predominantly Eocene age extends from Anatolia into Iran representing a major magmatic flare-up. We present new zircon U-Pb, Ar/Ar mica and apatite fission-track ages for this magmatism from northwestern Turkey, and review its geochemistry and geodynamic setting. The new age data show that magmatism started at the Late Paleocene (58 Ma) during the final stages of continental collision and continued into the early Middle Eocene (45 Ma) with most of the magmatism taking place in the Early-Middle Eocene (54 to 45 Ma). The Late Paleocene-Middle Eocene magmatism is separated from Late Cretaceous and Oligo-Miocene magmatic flare-ups by periods of magmatic quiescence. The Late Paleocene-Middle Eocene magmatism consists of plutonic and volcanic belts. The plutonic belt cuts across and post-dates the İzmir-Ankara suture. The plutonic rocks are mainly middle- to high-K calc-alkaline I-type granodiorite and granite, and the volcanic rocks are middle- to high-K calc-alkaline basalt, basaltic andesite and andesite. Geochemically, all the rocks are similar to those found in subduction-related environments. Crustal thicknesses calculated based on geochemistry suggest a thickened crust (60–70 km) at 58 to 54 Ma, and a relatively thin crust (ca. 40 km) at 54 to 45 Ma, which match with uplift and erosion during the Late Paleocene, and marine sedimentation during the Early-Middle Eocene in northwest Anatolia, respectively. The Late Paleocene-Middle Eocene magmatism is tentatively assigned to subduction of the southern branch of the Neo-Tethys.

1. Introduction

Geochronological data on magmatic rocks in concert with their areal distribution in Western Anatolia indicate three temporally and spatially distinct magmatic flare-ups separated by magmatic lulls (Figs. 1 and 2). These are Late Cretaceous (90–75 Ma), Late Paleocene–Middle Eocene (58–45 Ma) and Late Oligocene–Early Miocene (28–20 Ma) magmatic episodes (e.g., Okay et al., 2020a; Schleiffarth et al., 2018). The Late Cretaceous magmatic belt is part of a major magmatic arc extending from Georgia in the east to Serbia in the west (e.g., Gallhofer et al., 2015; Moritz et al., 2020). It formed as a result of northward subduction of the Tethyan ocean under the Pontides. The İzmir-Ankara-Erzincan suture represents the trace of this İzmir-Ankara ocean, which is also known as the northern branch of the Neo-Tethys (Fig. 1). The İzmir-Ankara ocean separated the Pontides from the Anatolide-Tauride Block during the Mesozoic and closed during the Paleocene. There was another Mesozoic-

Cenozoic ocean farther south between the Anatolide-Tauride Block and the Arabian Plate known as the southern branch of Neo-Tethys (e.g., Robertson et al., 2013). The partial closure of this ocean during the Miocene created the Bitlis-Zagros suture (Fig. 1b, Okay et al., 2010), the Eastern Mediterranean represents a relict of the southern branch of Neo-Tethys.

The Late Paleocene-Middle Eocene magmatism, abbreviated as LP-ME magmatism, is observed in the Pontides, as well as in the Anatolide-Tauride Block, and extends ~30–50 km south of the İzmir-Ankara-Erzincan suture (Fig. 1). The Late Oligocene–Early Miocene magmatic rocks generally crop out farther south and show a substantially wider aerial distribution in western Anatolia than the LP-ME ones (Fig. 1). The origin of the LP-ME magmatism is controversial and has been attributed to slab breakoff (Altunkaynak et al., 2012; Altunkaynak and Dilek, 2013; Ersoy et al., 2017; Ersoy and Palmer, 2013; Gülmez et al., 2013; Güraslan and Altunkaynak, 2019; Karacık et al., 2008;

* Corresponding author.

E-mail addresses: okay@itu.edu.tr (A.I. Okay), topuzg@itu.edu.tr (G. Topuz), kylander@geol.ucsb.edu (A.R.C. Kylander-Clark), Sarah.Sherlock@open.ac.uk (S. Sherlock), massimiliano.zattin@unipd.it (M. Zattin).

<https://doi.org/10.1016/j.lithos.2022.106816>

Received 27 March 2022; Received in revised form 23 July 2022; Accepted 27 July 2022

Available online 30 July 2022

0024-4937/© 2022 Elsevier B.V. All rights reserved.

Kasapoğlu et al., 2016; Keskin et al., 2008), delamination of the lower part of the thickened lithosphere (Köprübaşı and Aldanmaz, 2004) and subduction (Okay and Satır, 2006; Rabayrol et al., 2021; Ustaömer et al., 2009).

This paper deals with the LP-ME magmatic flare-up in northwestern Anatolia. We present new U-Pb zircon, Ar/Ar mica and apatite fission-track ages from a large number of LP-ME plutons (Table 1), and discuss these data in conjunction with the literature data on the distribution, duration, geochemistry and possible causes of the LP-ME magmatism in northwestern Turkey. Our reassessment demonstrates that the LP-ME magmatism was active between 58 Ma and 45 Ma with most of

the magmatism occurring in the Early-Middle Eocene (54 to 45 Ma, Fig. 2). Magmatism started when the continental crust was thick, continued during the Early-Middle Eocene extension, and ended with the whole scale uplift of Anatolia at the end of the Middle Eocene. The evidence for the Late Paleocene - Middle Eocene magmatic flareup is based on the age and spatial distribution of the magmatic rocks (Figs. 1, 2); calculation of a meaningful magmatic flux is not possible because: a) Large parts of western Anatolia are covered by the Neogene deposits (cf. Fig. 3), which disguises the true extent of magmatism, b) There has been extensive exhumation during the Cenozoic, as shown by the apatite fission track ages (Okay et al., 2020a), which eroded a significant part of



Fig. 1. a) Tectonic map of northern Aegean and northwest Anatolia showing the distribution of Late Cretaceous, Eocene and Oligo-Miocene magmatism. b) Tectonic map of the Middle East showing the distribution of the Eocene magmatism. For the Cenozoic isotopic ages in the Rhodopes see the compilations in Marchev et al. (2005) and Perkins et al. (2018).

the Eocene volcanic rocks, c) The thickness of the Eocene volcanic rocks varies over short distances, because of post-Eocene tectonism, and is poorly constrained.

2. Tectonic setting of the Late Paleocene – Middle Eocene magmatism

The LP-ME magmatism in central and northwestern Anatolia is found both in the Pontides and in the northern part of the Anatolide-Tauride Block, straddling the İzmir-Ankara-Erzincan Tethyan suture (Figs. 1 and 3). The Cenozoic magmatic belt extends eastwards into the Eastern Pontides and into the Lesser Caucasus, where it is also found on both sides of the suture (e.g., Kaygusuz et al., 2020; Moritz et al., 2020; Topuz et al., 2011). It continues into Iran as the Urumieh-Dokhtar magmatic arc north of the main Zagros suture, where the magmatic flare-up is dated between 53 Ma and 37 Ma (e.g., Mokhtari et al., 2022; Stern et al., 2021). The Cenozoic magmatic belt has a length of about 3000 km (Fig. 1b). Although the magmatic rocks in this long belt have a similar subduction-related geochemistry, there are temporal changes along the belt. The Late Paleocene magmatic rocks appear to be restricted to

northwest Turkey and Iran (e.g., Nouri et al., 2021). The prominent late Middle Eocene – Early Oligocene magmatic lull (45–28 Ma) of the Pontides is not observed in the Lesser Caucasus and in the Urumieh-Dokhtar belt (e.g., Grosjean et al., 2022).

The İzmir-Ankara-Erzincan suture in northern Turkey marks the trace of a middle Paleozoic – Mesozoic Tethyan ocean, which closed by northward subduction under the Pontides followed by a collision between the Anatolide-Tauride Block and the Pontides in the Paleocene (e.g., Mueller et al., 2019). Therefore, the LP-ME magmatism is post-tectonic with respect to the closure of the İzmir-Ankara ocean.

The LP-ME magmatism in northwest Turkey is represented by plutonic and volcanic rocks. The plutons form a 410-km-long and 40 km wide belt extending from the central Anatolia to the Marmara region, roughly parallel to the Eskişehir Fault, which is a major Late Eocene - Oligocene dextral strike-slip fault (Fig. 1, Okay et al., 2008). After a gap represented by the Upper Eocene-Miocene sedimentary rocks of the Thrace basin, Eocene granites crop out in the Rhodopes in eastern Greece and Bulgaria (Fig. 1, e.g., Marchev et al., 2013). The magmatism in the Rhodopes is different from the main LP-ME magmatic belt in that there is no spatial or temporal separation of the LP-ME and Oligo-

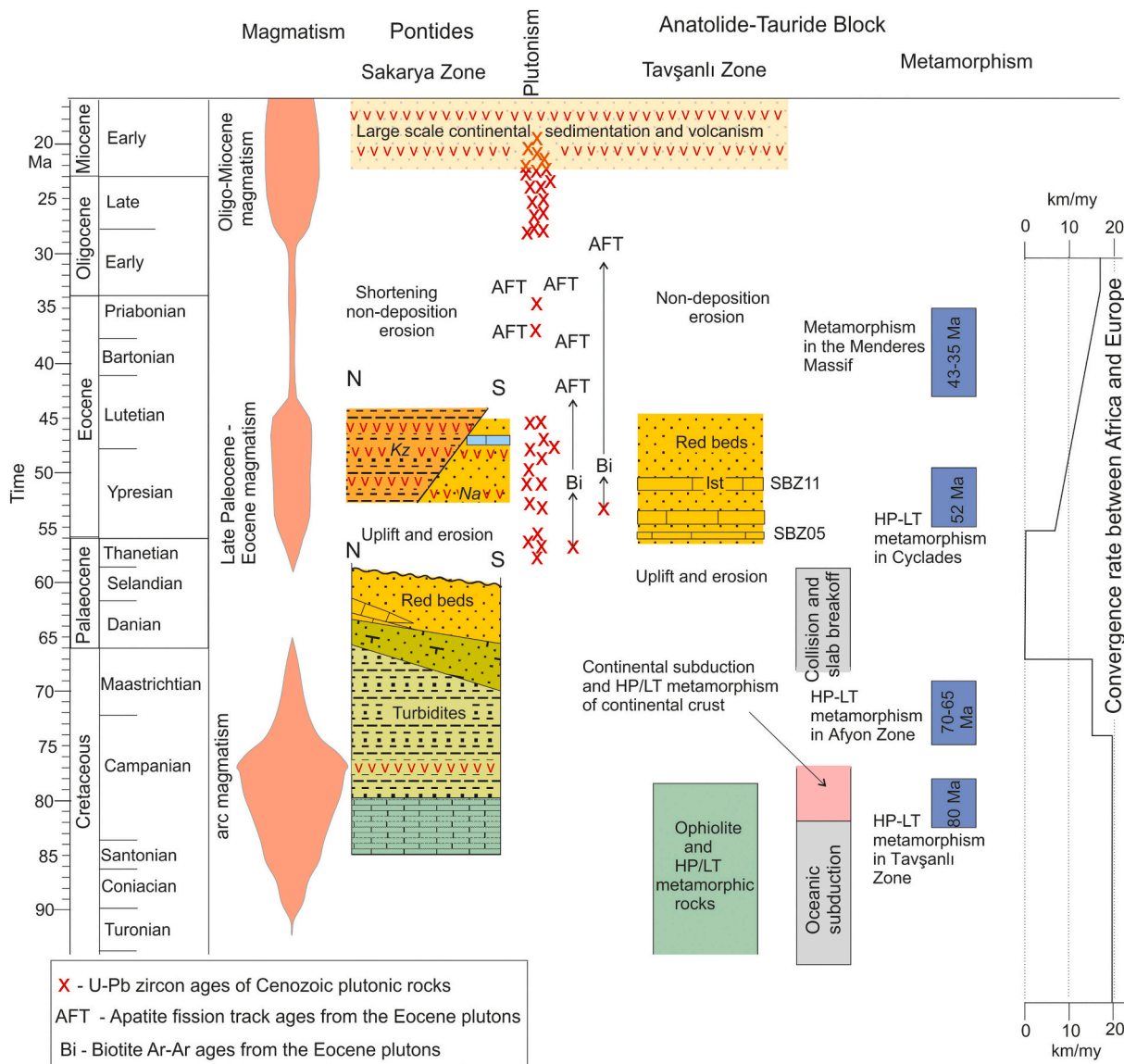


Fig. 2. Late Cretaceous to late Cenozoic magmatism, sedimentation and tectonic events in northwest Turkey. Also shown is the convergence rate between Africa and Eurasia after Smith (2006). Kz, Kızderbent volcanics; Na, Nallıhan volcanics; SBZ, shallow benthic zones.

Table 1
Zircon U-Pb and Ar/Ar mica age data from northwest Anatolia.

New zircon U-Pb ages from magmatic rocks						
Name	Sample number	Rock type	Age (Ma)	Number of concordant ages	Number of inherited ages	Stratigraphic age
	12410	granitoid	48.0 ± 0.4	31	0	Early Eocene
Fıstıklı (Fs)	12422	granitoid	48.0 ± 0.5	35	0	Early Eocene
Kadıncık (Kd)	9384	granitoid	56.6 ± 0.4	33	3	Late Paleocene
Karacaören (Ka)	9413	granitoid	54.7 ± 3.1	39	0	Early Eocene
Kaymaz (Ky)	9429	granitoid	55.3 ± 1.2	22	0	Early Eocene
Sivrihisar (Sv)	9404	granitoid	55.3 ± 0.3	57	0	Early Eocene
Tekören (Tk)	8876	granitoid	57.6 ± 0.8	23	0	Late Paleocene
Topkaya (Top)	9431	granitoid	45.3 ± 0.2	42	1	Early Middle Eocene (Lutetian)
Sivrihisar - dyke	10372	granitoid	56.6 ± 0.6	3	0	Latest Paleocene
Block in Eocene sandstone	10048	dacite-porphyr	45.7 ± 0.4	43	5	Early Middle Eocene (Lutetian)
Kızderbent volcanics	14396	tuff	48.0 ± 0.7	33	0	Early Eocene

Published zircon U-Pb ages from the Eocene magmatic rocks from northwest Anatolia					
Name of the intrusion	Rock type	Reference	Age (Ma)	Stratigraphic age	
Asartepe (As)	Granitoid	Akgündüz et al., 2012	47.0 ± 1.1	Early Middle Eocene (Lutetian)	
Ekmekçi (EK)	Granitoid	Sunal et al., 2019	50.9 ± 1.2	Early Eocene	
Gürgenyayla (Gy)	Granitoid	Altunkaynak et al., 2012, Rabayrol et al., 2021	51.0 ± 0.5 51.5 ± 0.1	Early Eocene	
Karabiga (Kb)	Granitoid	Altunkaynak et al., 2012	47.0 ± 0.8	Early Middle Eocene (Lutetian)	
Marmara Island (Mr)	Granitoid	Ustaömer et al., 2009	47.6 ± 2.0	Early-Middle Eocene boundary	
Orhaneli (Or)	Granitoid	Altunkaynak et al., 2012	52.8 ± 1.8	Early Eocene	
Tepeldağ (Tep)	Granitoid	Okay and Satır, 2006 Altunkaynak et al., 2012	45.0 ± 0.2 45.4 ± 0.3	Early Middle Eocene (Lutetian)	
Topuk (Tp)	Granitoid	Altunkaynak et al., 2012	48.7 ± 0.4	Early Eocene	
Sivrihisar (Sv)	Granitoid	Özdamar et al., 2018, Rabayrol et al., 2021	50.5 ± 0.3, 55.2 ± 0.6	Early Eocene	
South Kapıdağ (SKp)	Granitoid	Altunkaynak et al., 2012	36.8 ± 0.7	Late Eocene	
Yürükkaracaören	Granitoid	Rabayrol et al., 2021	48.2 ± 0.5	Early Eocene	
Nallihan volcanics	Andesite tuff	Kasapoğlu et al., 2016 Mueller et al., 2019	48–52	Early Eocene	

New Ar-Ar mica ages						
Unit	Lithology	Dated mineral	No. of grains dated	Numeric age	Stratigraphic age	Sample number
Günyüzü metamorphics	Micaschist	Biotite	6	25.7 ± 1.7	Late Oligocene	8877
Günyüzü metamorphics	Micaschist	Muscovite	6	49.8 ± 1.0	Early Eocene	8877
Günyüzü metamorphics	Micaschist	Muscovite	12	84.3 ± 2.3	Late Cretaceous	10131
Günyüzü metamorphics	Micaschist	Muscovite	16	109.0 ± 2.7	Early Cretaceous	10139
Kadıncık (Kd)	Granite	Biotite	12	51.0 ± 0.6	Early Eocene	9384
Karacaören (Ka)	Granite	Biotite	12	49.3 ± 1.1	Early Eocene	9413

Miocene magmatic rocks, and the magmatism appears to be continuous from earliest Eocene into Miocene (Fig. 1).

In northwest Turkey, there are at least twenty LP-ME plutons of varying sizes. The real extent of the LP-ME plutonism is greater since large parts of this region are covered by Neogene deposits (Fig. 3). The Early to Middle Eocene volcanic rocks crop out north of the plutonic belt in a roughly E-W direction and the magmatism extends eastwards to the Eastern Pontides, Lesser Caucasus and Iran (e.g., Arslan et al., 2013; Kaygusuz et al., 2020; Keskin et al., 2008; Moritz et al., 2020; Stern et al., 2021; Topuz et al., 2011). In the west the LP-ME plutonic belt and the Early to Middle Eocene volcanic belt merge in the Armutlu Peninsula. The width of the LP-ME magmatic belt ranges between 120 and 180 km in northwestern Turkey (Fig. 1).

The LP-ME plutons intrude the blueschists and ophiolites of the Tavşanlı Zone of the Anatolide-Tauride Block and the pre-Jurassic basement of the Pontides. The Tavşanlı Zone represents the northern margin of the Anatolide-Tauride Block, which was subducted during the Late Cretaceous (e.g., Plunder et al., 2015). The blueschist metamorphism is dated to ca. 80 Ma and affects both continental and oceanic lithologies (Sherlock et al., 1999). The Tavşanlı blueschists are tectonically overlain by ophiolitic mélanges and by ophiolites, which are locally unconformably overlain by Lower and Middle Eocene continental and marine sedimentary rocks (Özgen-Erdem et al., 2007).

3. Analytical methods

Methods employed during this study include U-Pb and Ar/Ar geochronology and apatite fission-track (AFT) thermochronology. Mineral separation was done in the Istanbul Technical University using classical techniques including crushing, sieving, and magnetic separation. For zircon and apatite separation we used sodium polytungstate as a heavy liquid. The zircons were picked under a stereographic microscope and mounted in epoxy and were polished in the Istanbul Technical University. Cathodoluminescence imaging of the zircon internal structures was carried out at the Geological Department of the Hacettepe University (Ankara). The zircons were analyzed using laser ablation inductively coupled plasma mass spectrometry (LA-ICP-MS) at the University of California, Santa Barbara. For the details of the method employed, see Okay et al. (2020b). Long-term reproducibility in secondary reference materials is <2% and, as such, should be used when comparing ages obtained within this analytical session to ages elsewhere. Mica samples were dated using the Ar/Ar single-grain fusion method at the Open University in the United Kingdom. For the details of the method see Okay et al. (2020b). The U-Pb and Ar/Ar analytical data are given in supporting information Tables S1 and S2, respectively. The AFT analyses were carried out at the Department of Biological, Geological and Environmental Sciences of the University of Bologna, Italy. For the AFT analysis the final selection of the apatite grains were done by hand-picking under a binocular stereographic microscope.

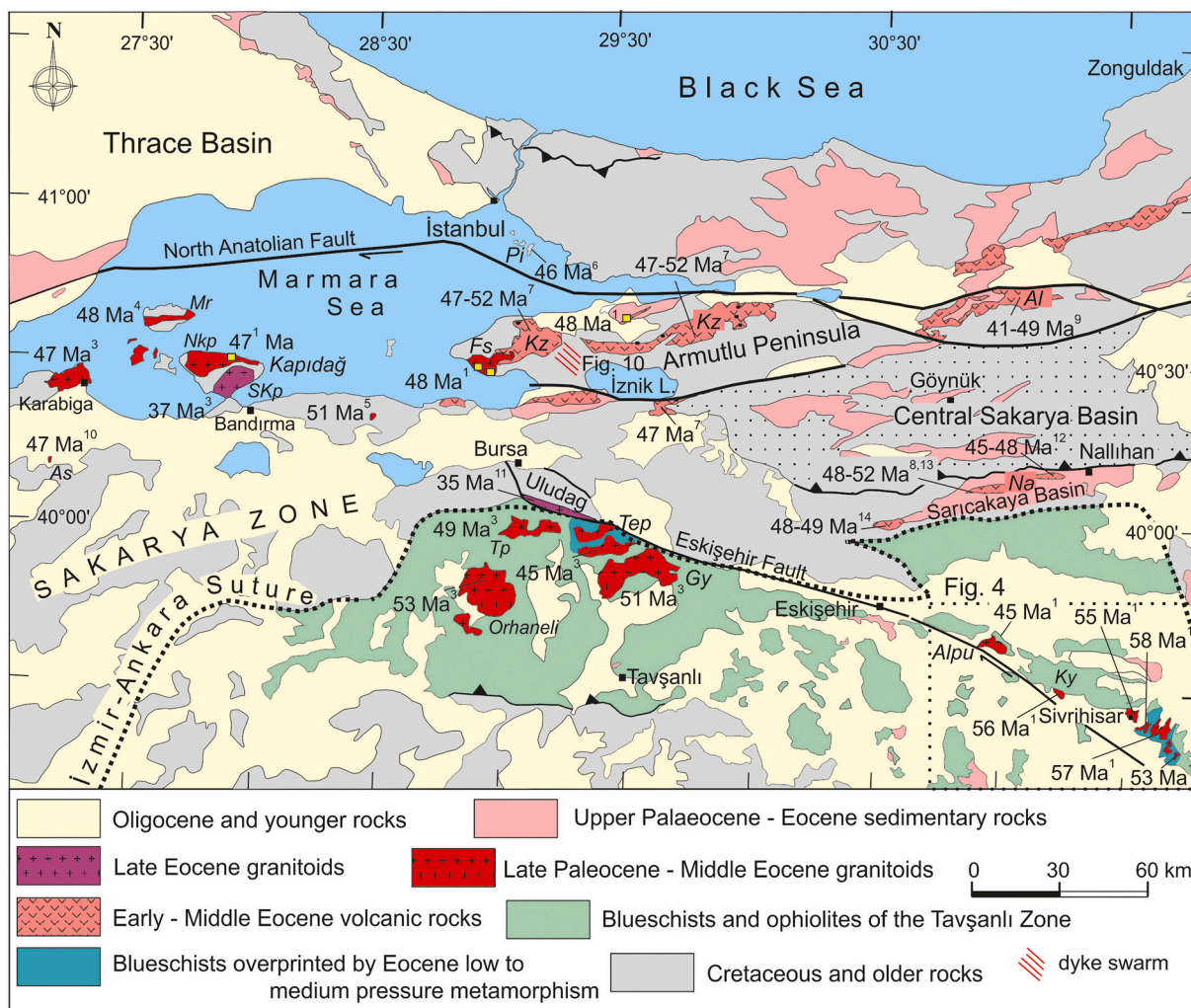


Fig. 3. Geological map of northwestern Turkey and northern Aegean showing the distribution and ages of the Late Paleocene - Eocene magmatic rocks. *Al* Almacık; *Bz* Bozaniç; *Fs* Fıstıklı; *Gy* Gürgenyayla; *Kb* Karabiga; *Ky* Kaymaz; *Kz* Kızderbent; *Mr* Marmara; *Na* Nallıhan; *Nkp* North Kapıdağ; *Pi* Princes Island; *Skp* South Kapıdağ; *Tep* Tepeladağ; *Tp* Topuk. The sources for the ages are: 1. This study, 2. Ersoy et al., 2017, 3. Altunkaynak et al., 2012, 4. Ustaömer et al., 2009, 5. Sunal et al., 2019, 6. Şen, 2020, 7. Kürkçüoğlu et al., 2008, 8. Kasapoğlu et al., 2016, 9. Gülmez et al., 2013, 10. Akgündüz et al., 2012, 11. Topuz and Okay, 2017, 12. Şahin et al., 2019, 13. Mueller et al., 2019, 14. Büyükkahraman, 2016.

Apatite grains were mounted in epoxy resin, ground, and polished to expose planar surfaces within the grains and then etched with 5N_{HNO}3 at 20 °C for 20 s to reveal the spontaneous tracks. Apatite fission-track age data are reported as central ages, a weighted modal age calculated through an iterative algorithm.

4. Late Paleocene-Middle Eocene plutonic rocks and their geochemical features

In central and northwest Turkey, the LP-ME plutons occur in three clusters: Sivrihisar – Günyüzü, Western Tavşanlı Zone and Southern Marmara (Figs. 1 and 3). Geochemical and isotopic characteristics from literature as well as field relations and our new geochronological data are summarized below.

4.1. The Sivrihisar – Günyüzü Plutons

There are about six plutons in this region all intruding the metamorphic rocks of the Tavşanlı Zone (Fig. 4, Kibici et al., 2008; Shin et al., 2013; Demirbilek et al., 2018; Bağcı et al., 2019). The closely spaced plutonic bodies between Günyüzü and Sivrihisar are probably connected at depth. All the plutons form prominent features in the landscape and

intrude the micaschists and marbles of the Tavşanlı Zone (Fig. 5a, b); intrusive veins and dykes are common in the metamorphic rocks (Fig. 5c). Around the Sivrihisar-Günyüzü plutons, blueschist-facies metamorphic rocks of the Tavşanlı Zone were overprinted by an Eocene high-temperature/low-pressure metamorphism (Fig. 3, Whitney et al., 2011; Seaton et al., 2013).

The Sivrihisar-Günyüzü plutons are mainly medium-grained biotite-hornblende-bearing granodiorites and granites with subordinate monzonite, quartz-monzonite and syenite (Fig. 6a, Kibici et al., 2008; Shin et al., 2013; Demirbilek et al., 2018; Bağcı et al., 2019). The Sivrihisar Pluton consists of monzonite and the Dinek intrusion is largely quartz-monzonite. Some of the intrusive bodies contain several centimeter large K-feldspar crystals (e.g., Dinek, Karacaören, Fig. 5d). Geochemical data from the literature (Table S3; Kibici et al., 2008; Shin et al., 2013; Demirbilek et al., 2018; Bağcı et al., 2019) indicate that the granodiorites and granites belong to middle- to high-K calc-alkaline series, and monzonites and quartz-monzonites mainly to shoshonitic series on the SiO₂ vs. K₂O diagram of Peccerillo and Taylor (1976) (Fig. S1a). Rocks of the Sivrihisar-Günyüzü plutons fall into the calcic, calc-alkalic, alkali-calcic and minor alkalic fields based on the modified alkali-lime index [(Na₂O+K₂O)-CaO] defined by Frost et al. (2001) (Fig. S2a). Even the rocks from a single intrusive body, e.g., the Karacaören

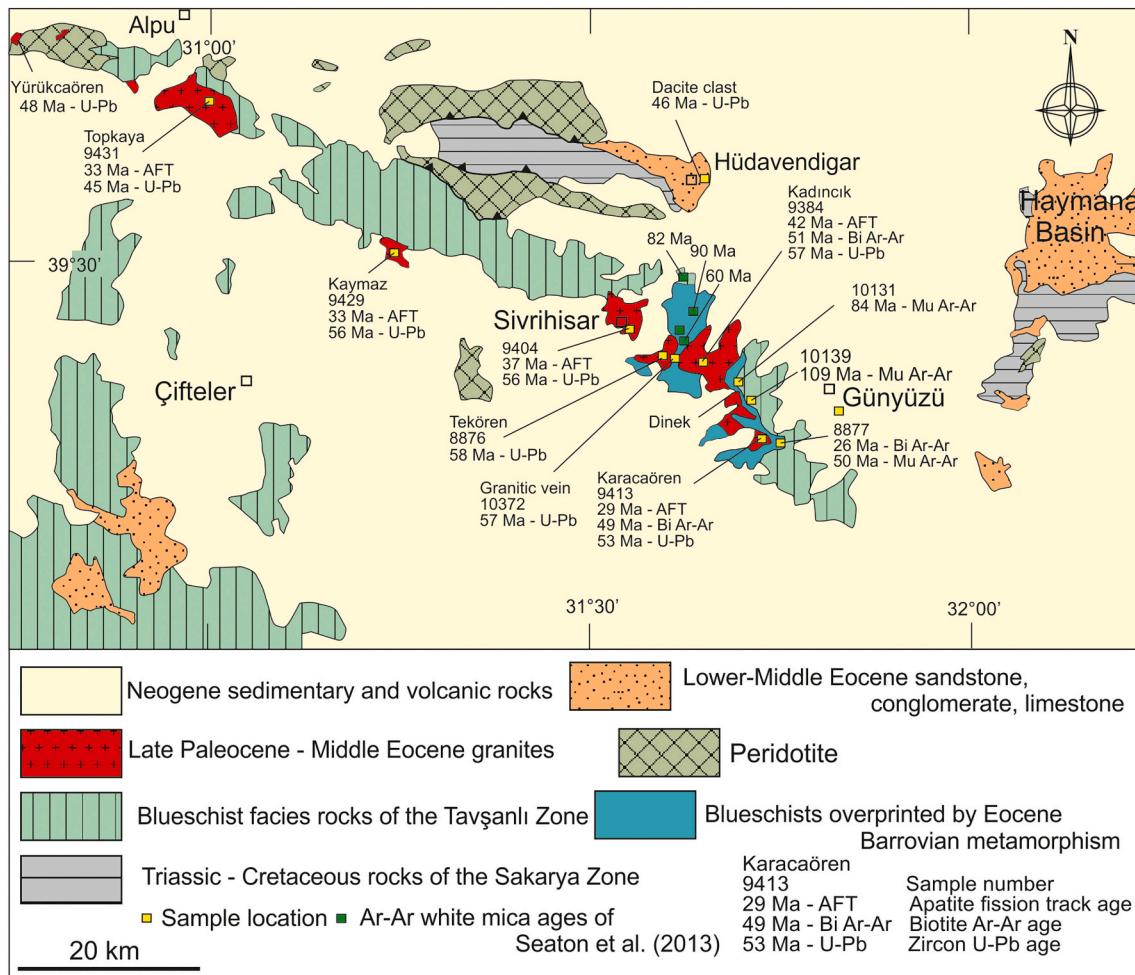


Fig. 4. Geological map of the Sivrihisar – Günyüzü area in central Anatolia showing the distribution of the Cenozoic granites and the new isotopic ages (based on Demirbilek et al. (2018) and our mapping). For location see Fig. 3.

Pluton, show a large scatter on the SiO_2 vs. $[(\text{Na}_2\text{O}+\text{K}_2\text{O})-\text{CaO}]$ diagram, which can be explained by the composite nature of the pluton and/or by the difficulty of obtaining representative compositions from granites with several centimeter-large feldspar crystals (Fig. 5d). On the multi-element variation diagrams normalized to the primitive mantle after Sun and McDonough (1989), the rocks from the Sivrihisar-Günyüzü plutons display enriched large ion lithophile elements and negative anomalies of Nb-Ta, Sr and Ti, similar to the rocks formed in subduction-related environments (Bağcı et al., 2019; Demirbilek et al., 2018; Kibici et al., 2008). Chondrite-normalized rare earth element patterns of the samples from the Sivrihisar-Günyüzü plutons are variably steep, and display variably negative Eu anomalies (Fig. S3). The samples from the plutons with igneous crystallization ages younger than 54 Ma tend to have less steep REE patterns ($(\text{La}/\text{Yb})_{\text{cn}} < 15$) than those older than 54 Ma ($(\text{La}/\text{Yb})_{\text{cn}} > 15$, Fig. S3). Samples from the Karacaören Pluton have variable $(\text{La}/\text{Yb})_{\text{cn}}$ and Eu/Eu^* ratios ($(\text{La}/\text{Yb})_{\text{cn}} = 2.84\text{--}13.77$; $\text{Eu}/\text{Eu}^* = 0.30\text{--}1.56$). Initial $^{87}\text{Sr}/^{86}\text{Sr}$ and ϵNd values of the plutons are 0.7053–0.7068 and 0.23 to –2.92, respectively (Fig. 7a, Table S4, Demirbilek et al., 2018). Only samples of the Kaymaz Granite display significantly different initial $^{87}\text{Sr}/^{86}\text{Sr}$ and ϵNd values (initial $^{87}\text{Sr}/^{86}\text{Sr} = 0.7097\text{--}0.7100$; initial $\epsilon\text{Nd} = -6.17$ - -6.49). There is no apparent relationship between the isotopic composition, age and lithology of the plutons.

We have dated zircons from six intrusions and a dyke from the Sivrihisar – Günyüzü plutons; the U-Pb zircon crystallization ages of the plutons range from Late Paleocene (58 Ma) to Middle Eocene (45 Ma, Fig. 8, Tables 1 and S3) and they include the oldest intrusions of the

Paleocene-Eocene plutonic belt. The dates are based on concordant zircon U-Pb ages from 271 grains from six intrusions and a granitic dyke; remarkably, inherited zircons are limited only to four grains in two samples (Table 1 and Table S1). The closely spaced plutons between Sivrihisar and Günyüzü have ages between 58 and 53 Ma (Fig. 8). Zircons from a one-meter-thick granitic dyke vein cutting the marbles (sample 10372) also produced a Late Paleocene age of 56.6 ± 0.6 Ma (Fig. 9). The Sivrihisar Monzonite gave a zircon U-Pb age of 55.3 ± 0.2 Ma based on 57 zircon grains, which is compatible with its 55.2 ± 0.6 Ma zircon U-Pb age reported by Rabayrol et al. (2021) but older than the 50.6 ± 0.3 Ma U-Pb zircon age reported by Özdamar et al. (2018). The very scattered U-Pb zircon ages reported by Shin et al. (2013) from the Sivrihisar Monzonite are most likely an artifact of the in situ dating in thin section, especially considering that all of the 109 concordant zircon ages from the Sivrihisar Monzonite from our data, from Rabayrol et al. (2021) and from Özdamar et al. (2018) fall in the range of 49 Ma to 56 Ma.

The Kaymaz Granite is a small body intruding metamorphic rocks and serpentinite; gold and silver are mined in the silicified serpentinite at the contact with the granite (Rabayrol et al., 2021). The Kaymaz Granite has yielded an Early Eocene U-Pb zircon age of 55.3 ± 1.2 Ma (Fig. 8); all the dated zircons are Early Eocene with no inherited zircon grains. The Topkaya Granodiorite is a poorly exposed intrusion south of Alpu (Fig. 3), and has yielded an early Middle Eocene (Lutetian) age of 45.3 ± 0.2 Ma (Fig. 8).

We also determined biotite Ar/Ar ages from the Kadıncık and Karacaören granitoids in the Günyüzü area, to constrain the cooling of the



Fig. 5. Field photographs of the Late Paleocene – Middle Eocene magmatic rocks from the Sivrihisar-Günyüzü plutons. a. Tekören Granodiorite intruding the marbles and schists of the Tavşanlı Zone in the Sivrihisar-Günyüzü area. b. Sivrihisar Monzonite. c. Granitic veins cutting the schists in the Günyüzü area. d. Kadıncık granite with several centimeter large feldspar crystals.

plutons (Table 1 and S2). The biotite Ar/Ar ages are within five million years of the respective zircon U-Pb ages (56.5 Ma → 51.0 Ma and 52.7 Ma → 49.3 Ma, respectively). For the Sivrihisar Monzonite the zircon U-Pb and Ar/Ar hornblende ages are 55.2 and 53–51 Ma, respectively (Demirbilek et al., 2018; Sherlock et al., 1999). Demirbilek et al. (2018) also reported K-Ar hornblende, biotite and feldspar ages from the Sivrihisar – Günyüzü plutons, which are close to their crystallization ages. The Ar/Ar and K-Ar ages indicate fast cooling below ca. 300 °C after the crystallization of the Sivrihisar-Günyüzü plutons.

Sedimentary Eocene sequences crop out north and southwest of the Sivrihisar – Günyüzü plutons and lie unconformably over the metamorphic rocks and peridotite of the Tavşanlı Zone (Fig. 4). The Eocene sequence southwest of the plutons near Çifteler consists of several hundred meters thick shallow marine limestone of Early Eocene age (Fig. 2, Shallow Benthic Zones 5 to 11, 56–50 Ma, Özgen-Erdem et al., 2007). The Eocene sequence north of Sivrihisar consists predominantly of fluvial sandstone and conglomerate with rare marine sandy limestone intercalations. Large benthic foraminifera in different sandy limestone beds indicate Early (SBZ10, 53–51 Ma) and Middle Eocene (Lutetian, 48–41 Ma) ages (Fig. 2, Akkiraz et al., 2022). The conglomerate beds in the Eocene series contain well-rounded clasts of limestone,

marble, schist, dacite and andesite. We dated a 40-cm-large porphyritic dacite clast (sample 10,048) from a conglomerate bed to constrain the age of the continental sedimentation. Forty-three zircon grains gave a Middle Eocene (Lutetian) U-Pb age of 45.7 ± 0.4 Ma (Fig. 9), compatible with the paleontological data.

4.2. The Western Tavşanlı Zone Plutons

Four large plutons (Orhaneli, Topuk, Gürgenyayla and Tepeldağ) crop out in the western part of the Tavşanlı Zone south of Bursa (Figs. 1 and 3). Similar to the Sivrihisar-Günyüzü plutons, the Western Tavşanlı Zone plutons intrude the blueschist and ophiolite.

The Western Tavşanlı Zone plutons are petrologically and geochemically similar to the Sivrihisar – Günyüzü plutons and are represented mainly by hornblende-biotite granodiorite and granite with subordinate syenite, quartz-monzonite and monzonite (Fig. 6b, Harris et al., 1994; Altunkaynak et al., 2012; Güraslan and Altunkaynak, 2019; Özyurt and Altunkaynak, 2020). With the exception of the Orhaneli Pluton, all the plutons display a narrow compositional variation ranging from granodiorite to granite of middle to high-K calc-alkaline affinity (Fig. 6b). The Orhaneli Pluton, however, comprises diorite,

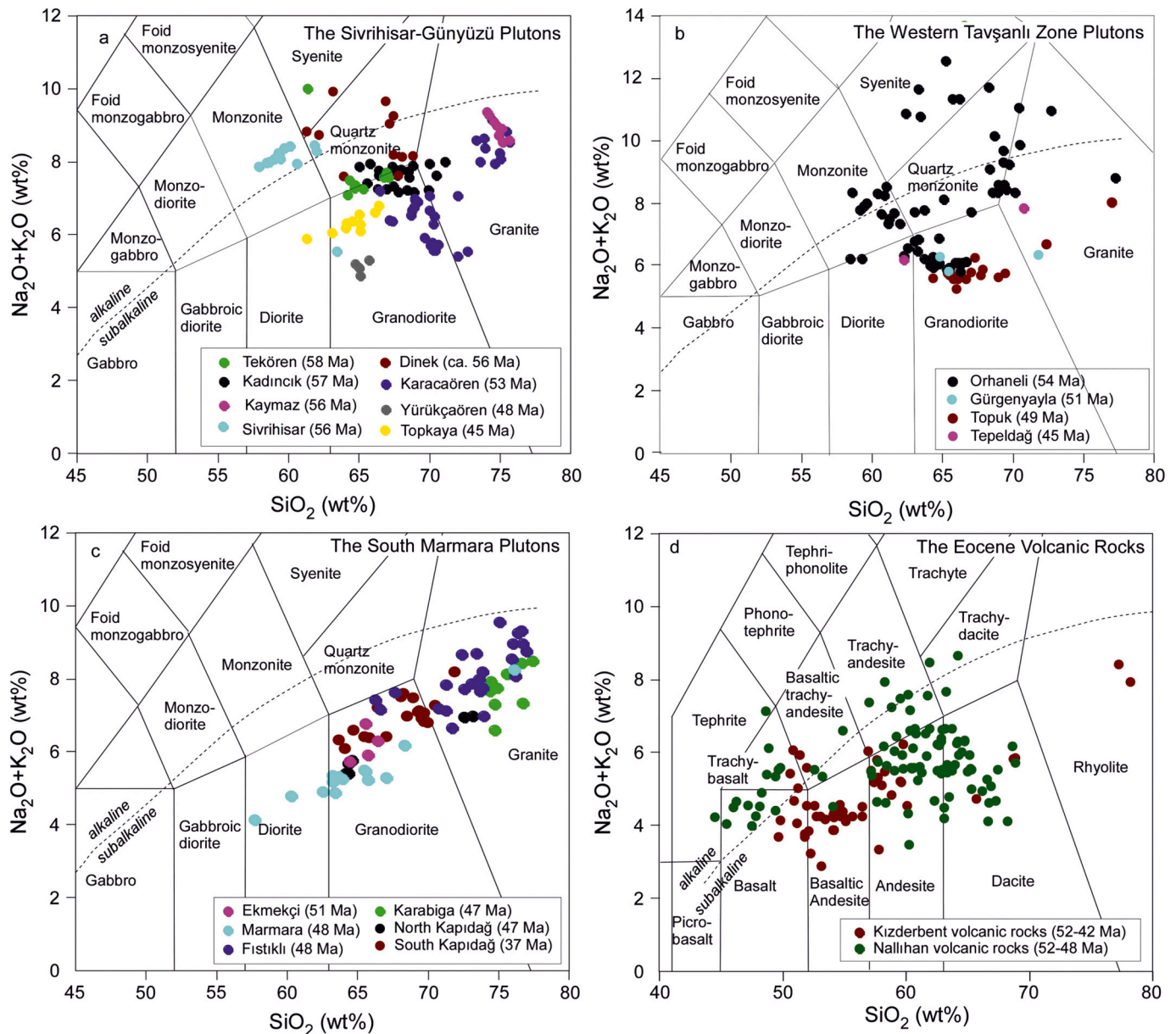


Fig. 6. Compositional variations of the Late Paleocene – Middle Eocene igneous rocks from the Western Anatolia in the diagram SiO_2 vs $\text{Na}_2\text{O} + \text{K}_2\text{O}$ diagram (after Middlemost, 1994). The division line (broken) for alkaline and subalkaline series is taken from Irvine and Baragar (1971). Data sources are given in the text.

granodiorite, granite, syenite, monzonite and quartz-monzonite, whereby quartz-monzonite occurs as dikes (e.g., Altunkaynak et al., 2012; Çelebi and Köprubaşı, 2014; Özyurt and Altunkaynak, 2020). Thus, rocks of the Orhaneli Pluton range from middle-K to high-K calc-alkaline to shoshonitic compositions, indicative of its composite nature (Fig. S1). According to the modified alkali-lime index $[(\text{Na}_2\text{O} + \text{K}_2\text{O}) - \text{CaO}]$, the Topuk, Gürgenyayla and Tepeldağ plutons are mainly calcic to locally calc-alkalic, while samples from the Orhaneli Pluton plot in the whole spectrum (Fig. S2). Overall, samples from the relatively younger plutons (51 to 45 Ma) such as Topuk, Gürgenyayla and Tepeldağ are characterized by relatively low chondrite-normalized La/Yb ratios (3–8), and variable negative Eu anomalies ($\text{Eu}/\text{Eu}^* = 0.45\text{--}1.00$) (Fig. S3b, Harris et al., 1994; Altunkaynak et al., 2012; Güraslan and Altunkaynak, 2019). However, rocks of the Orhaneli Pluton display a wide-ranging chondrite-normalized La/Yb ratios (5–84) and Eu anomalies ($\text{Eu}/\text{Eu}^* = 0.45\text{--}1.12$, Fig. S3, Altunkaynak et al., 2012; Çelebi and Köprubaşı, 2014; Özyurt and Altunkaynak, 2020). On the multi-element variation diagrams normalized to primitive mantle, the rocks from the

Western Tavşanlı Zone plutons are enriched in large ion lithophile elements and show negative anomalies of Nb-Ta, Sr and Ti, similar to the rocks formed in subduction-related environments. Despite highly variable rock types, the rocks of the Western Tavşanlı Zone are characterized by narrow initial $^{87}\text{Sr}/^{86}\text{Sr}$ and ϵNd values of 0.70524–0.70676 and 0.55–3.89, respectively (Fig. 7b; Table S4, Altunkaynak et al., 2012; Çelebi and Köprubaşı, 2014; Güraslan and Altunkaynak, 2019; Özyurt and Altunkaynak, 2020).

The U-Pb zircon crystallization ages of the Western Tavşanlı Zone plutons range from 53 Ma to 45 Ma (Early to early Middle Eocene, Table 1), and their Ar/Ar cooling ages are within a few million years of their crystallization ages (Altunkaynak et al., 2012; Harris et al., 1994; Kuşcu et al., 2019).

4.3. The South Marmara Plutons

Several large Eocene plutons crop out on the southern margin of the Marmara Sea and on the Marmara islands (Fig. 3, Köprubaşı and

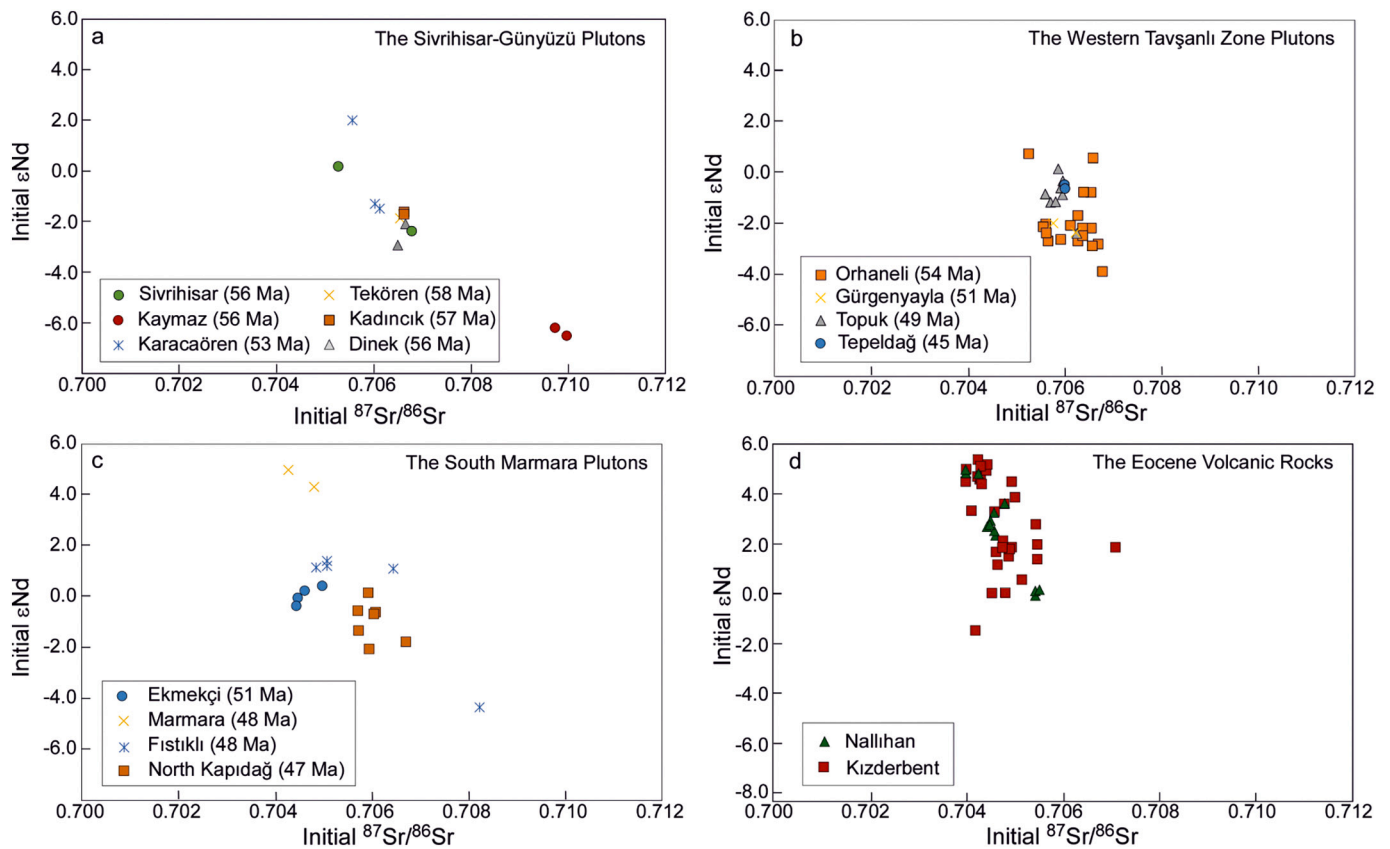


Fig. 7. Initial $^{87}\text{Sr}/^{86}\text{Sr}$ versus initial ϵNd values of Late Paleocene-Middle Eocene igneous rocks. Data are from Karacık et al. (2008), Kürkcüoğlu et al. (2008), Altunkaynak et al. (2012), Gülmez et al. (2013), Kasapoğlu et al. (2016), Büyükkahraman (2016), Demirbilek et al. (2018), Bağcı et al. (2019), Çelebi and Köprübaşı (2014), Gürarşlan and Altunkaynak (2019) and Özyurt and Altunkaynak (2020).

Aldanmaz, 2004; Karacık et al., 2008; Ustaömer et al., 2009; Altunkaynak et al., 2012; Sunal et al., 2019). The South Marmara plutons comprise mainly middle- to high-K calc-alkaline I-type granodiorite and granite, and minor diorite (Fig. 6, Köprübaşı and Aldanmaz, 2004; Karacık et al., 2008; Altunkaynak et al., 2012; Ustaömer et al., 2009; Sunal et al., 2019). In contrast to the Western Tavşanlı Zone and Sivrihisar-Günyüzü plutons, the South Marmara plutons do not contain any monzonite, syenite and quartz-monzonite. According to alkali lime index of Frost et al. (2001), the South Marmara plutons are calcic to calc-alkalic (Fig. S2c). Overall, rocks of the South Marmara plutons display variable chondrite-normalized La/Yb (3–14) and Eu/Eu^* (0.35–1.05) values (Fig. S3c, Köprübaşı and Aldanmaz, 2004; Altunkaynak et al., 2012; Sunal et al., 2019).

There are no published zircon U-Pb ages from the Fıstıklı Granite, which crops out on the Armutlu Peninsula, and the two published disparate K-Ar biotite ages are 48 and 35 Ma (Delaloye and Bingöl, 2000). We dated two samples from different parts of the Fıstıklı Granite (Fig. 1); they produced similar U-Pb zircon ages of 48.0 ± 0.4 and 48.0 ± 0.5 Ma (Fig. 9; Table 1 and S3), respectively, indicating crystallization during latest Early Eocene. There were no inherited zircons among the 66 grains dated. To constrain the temporal relation between plutonism and volcanism on the Armutlu Peninsula, we dated zircons from a 40-m-thick tuff bed in the northern part of the Armutlu Peninsula (sample 14396, Fig. 9). The tuff occurs within an Eocene sequence of turbiditic marine sandstone and shale (Fig. 10b, Özcan et al., 2012). An Early Eocene age 48.0 ± 0.7 Ma was obtained from the tuff bed based on 33 concordant zircon ages (Fig. 9), the same age as that of the Fıstıklı Granite. The age of the tuff also indicates that magmatism occurred during a time of marine sedimentation.

The North Kapıdağ Granite intrudes the Triassic metamorphic rocks of the Sakarya Zone. The northern margin of the pluton is deformed by a

shear zone and the granite in this region shows a strong planar fabric (Fig. 10a, Türkoğlu et al., 2016). Sample 7569 was collected from the shear zone; it yielded a U-Pb zircon age of 47.8 ± 1.1 Ma (Fig. 9), which falls on the Early-Middle Eocene boundary. This age also provides a lower age limit for the shear zone activity. Again, there were no inherited zircon grains among the dated zircon grains. The K-Ar biotite and hornblende ages from the North Kapıdağ Granite are in the range of 42–38 Ma (Delaloye and Bingöl, 2000).

The LP-ME magmatic flare-up ended at 45 Ma, and was followed by a magmatically quiet period until the Late Oligocene (ca. 28 Ma). In this respect, the South Kapıdağ intrusion, which has a Late Eocene U-Pb zircon age of 36.8 ± 0.7 Ma (Altunkaynak et al., 2012) is an exception. This age value is consistent with the Ar/Ar hornblende age of 36.0 ± 0.1 Ma (Altunkaynak et al., 2012) and K-Ar biotite age of 36–38 Ma (Delaloye and Bingöl, 2000) from the same intrusion. The South Kapıdağ Pluton is also geochemically different from the Middle Eocene South Marmara plutons, characterized by high chondrite normalized La/Yb ratios of 12–19 and a near absence of Eu anomaly (Fig. S3c, $\text{Eu}/\text{Eu}^* = 0.85\text{--}0.99$, Altunkaynak et al., 2012).

5. The Eocene volcanic rocks

The Eocene volcanic and volcanoclastic rocks crop out north of the plutonic belt in two east-west trending belts and are coeval with plutonism farther south (Figs. 1 and 3). The Kızderbent volcanic rocks crop out on the Armutlu Peninsula and in the Almacık region. They are intercalated with Lower and early Middle Eocene (Lutetian) marine sandstone, shale and marl (Özcan et al., 2012, Gülmez et al., 2013, Fig. 10b). The thickness of the Eocene sequence reaches 1500 m. Eocene andesite dykes are common and crosscut the metamorphic rocks and the Eocene volcanic rocks (Gülmez et al., 2013; Kürkcüoğlu et al., 2008). A

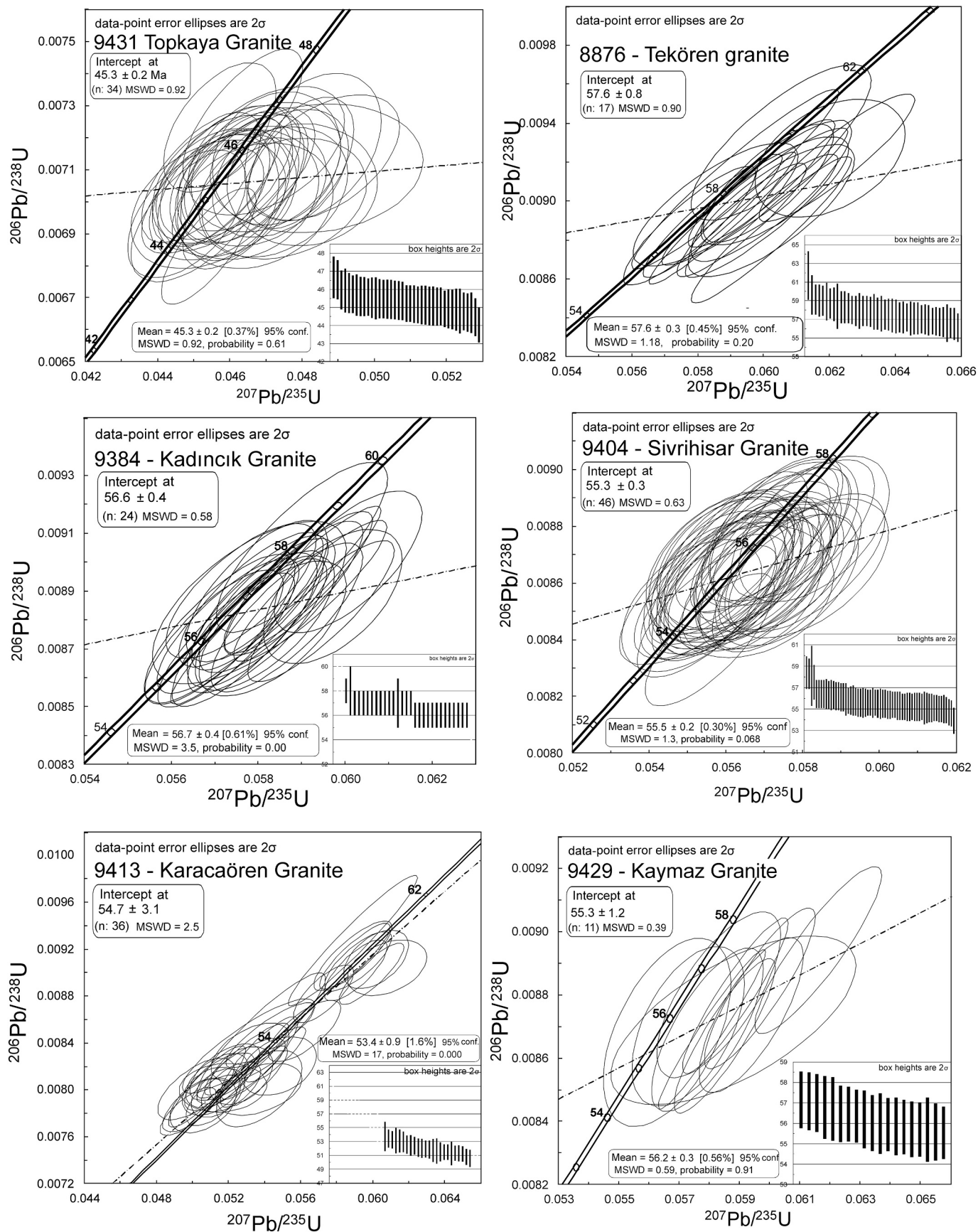


Fig. 8. Zircon U-Pb concordia diagrams from the Late Paleocene – Early Eocene granites. For data see Table S1.

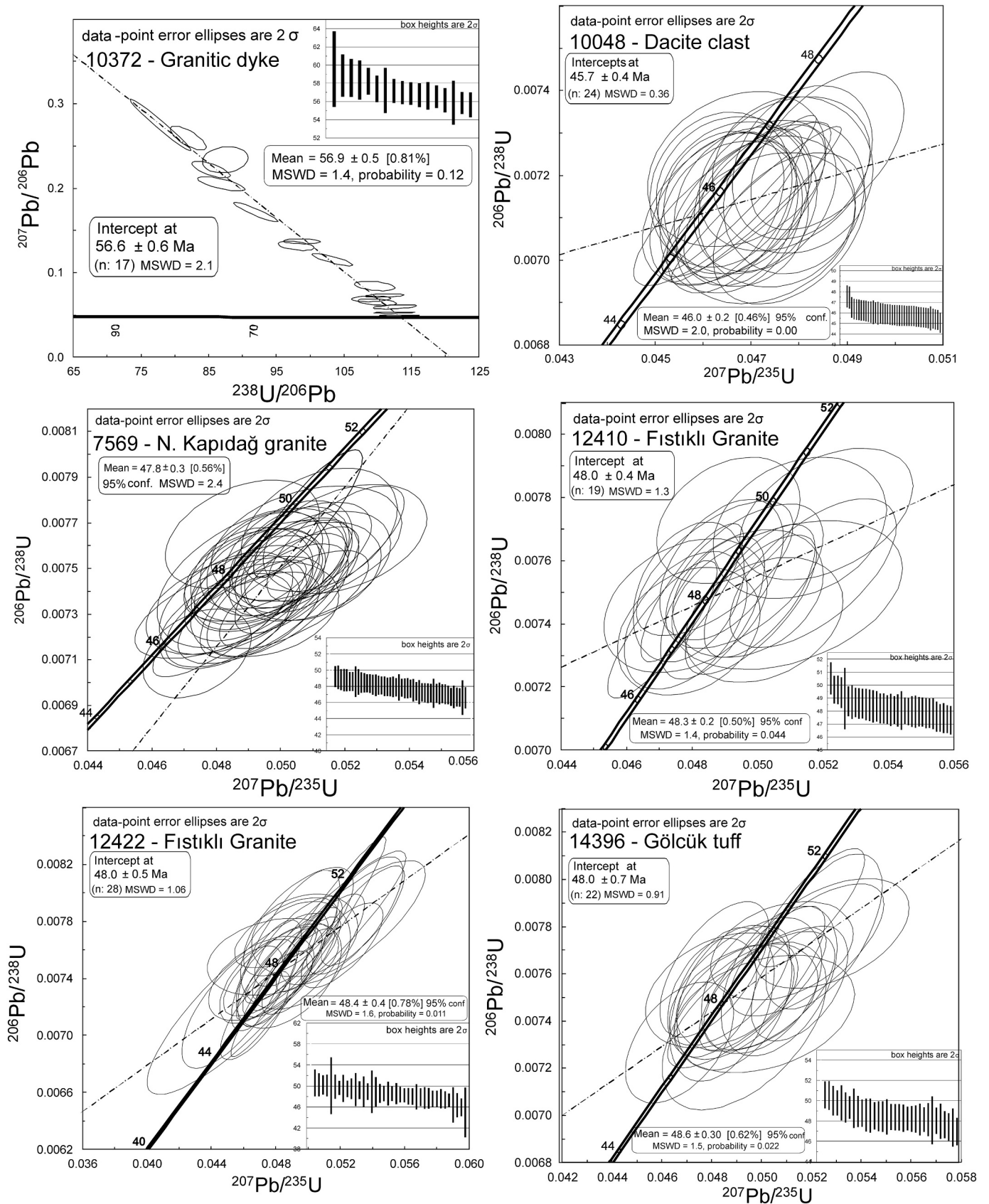


Fig. 9. Zircon U-Pb concordia diagrams from the Late Paleocene – Middle Eocene granites and volcanic rocks. For data see Table S1.

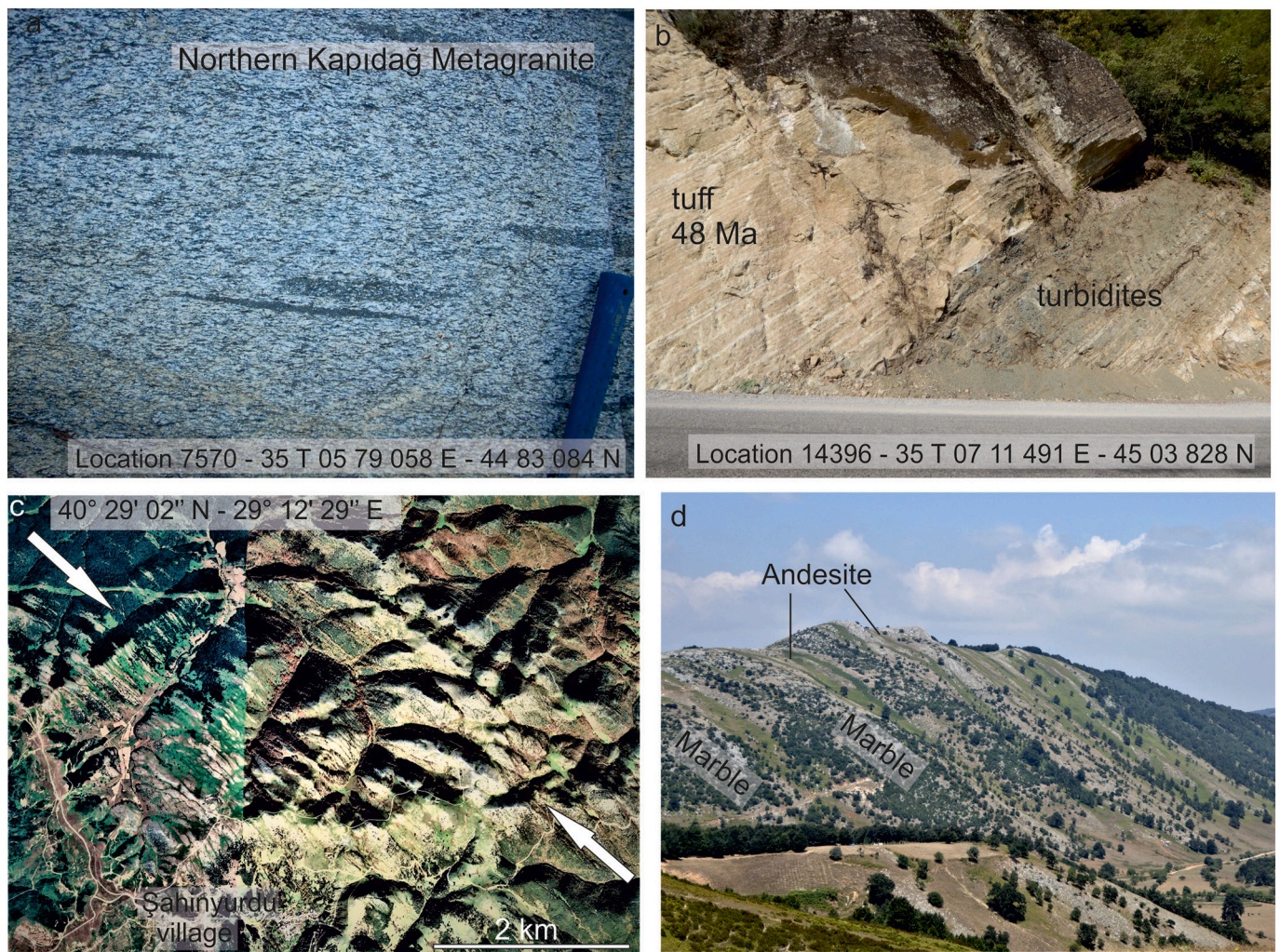


Fig. 10. Field photographs of the Eocene magmatic rocks. a. Sheared Northern Kapıdağ Granite. b. Lower Eocene tuff (sample 14396, 48.0 Ma) overlying siliciclastic marine turbidites. c. Google Earth image of the Eocene dyke swarm west of the İznik Lake on the Armutlu Peninsula. For location see Fig. 3. d. Field photo of the dyke swarm. Andesite dykes are less resistant to weathering than marble and form the green ribbons in c and d. (For interpretation of the references to colour in this figure legend, the reader is referred to the web version of this article.)

particularly dense dyke swarm with a width of 4 km cuts the marbles on the Armutlu Peninsula west of the İznik Lake (Fig. 10c, d). The dykes strike N42W and their width ranges from a few meters to tens of meters and they have lengths up to 8 km. The age of the Kızderbent volcanic rocks based on whole rock and mineral K-Ar and Ar/Ar dating ranges between 52 Ma and 42 Ma (Büyükkahraman, 2016; Gülmez et al., 2013; Kürkçüoğlu et al., 2008); a single zircon U-Pb age obtained in this study from a tuff bed is 48.0 ± 0.7 Ma (Figs. 9 and 10b).

In contrast to the Kızderbent volcanic rocks, which occur in an extensional marine setting, the Nallıhan volcanic rocks in the south are found in the Sarıcakaya foreland basin south of a major Eocene thrust fault (Fig. 3, Mueller et al., 2019; Şahin et al., 2019). The Nallıhan volcanic rocks are intercalated within a continental sequence of red sandstone and conglomerate (Şahin et al., 2019; Mueller et al., 2019) with rare shallow marine limestone beds of Middle Eocene age (SBZ13, ca. 44 Ma, Okay et al., 2020b). There are also small shallow-level intrusions. Zircon U-Pb ages from the Nallıhan volcanic rocks range between 52 Ma and 48 Ma (Kasapoğlu et al., 2016; Mueller et al., 2019).

A compilation of the literature data suggests that the Kızderbent and Nallıhan volcanic rocks consist predominantly of basaltic andesite and andesite and subordinate basalt, trachy-andesite, trachyte, dacite and rhyolite and their pyroclastic equivalents (Fig. 11a, Kürkçüoğlu et al., 2008; Gülmez et al., 2013; Yıldız et al., 2015; Büyükkahraman, 2016;

Kasapoğlu et al., 2016; Ersoy et al., 2017). They are variably altered as reflected in variable loss on ignition values (0.6–8.7 wt%, Table S3). The Eocene volcanic rocks display mainly a middle- to high-K calc-alkaline affinity, and a subordinate alkaline affinity (Figs. 10b and S1). The alkaline volcanic rocks appear to be confined to the Nallıhan area. All the volcanic rocks are characterized by narrow initial $^{87}\text{Sr}/^{86}\text{Sr}$ and ϵNd isotopic ratios (Fig. 7d, Kürkçüoğlu et al., 2008; Gülmez et al., 2013; Altunkaynak and Dilek, 2013; Kasapoğlu et al., 2016). The initial ϵNd values range from 5.40 to 0.50, and the initial $^{87}\text{Sr}/^{86}\text{Sr}$ values from 0.70390 to 0.70515. The alkaline volcanic rocks display nearly identical Sr and Nd isotopic compositions as the middle- to high-K calc-alkaline ones. The model ages calculated according to a depleted mantle range from 0.41 to 0.98 Ga; the majority is characterized by lower values of 0.44–0.75 Ga, which are significantly younger than those from the older granitoids (Büyükkahraman, 2016; Gülmez et al., 2013; Kasapoğlu et al., 2016; Kürkçüoğlu et al., 2008). All the volcanic rocks display geochemical features suggesting formation in subduction-related environments. However, the Nallıhan volcanic rocks tend to have much steeper REE patterns than the Kızderbent volcanic rocks with $(\text{La}/\text{Yb})_{\text{cn}}$ values of 5–15 and 2–5, respectively (Fig. S3).

Cenozoic volcanic rocks crop out over large areas in the Biga Peninsula (Fig. 1). Volcanism on the Biga peninsula is different than the rest of northwest Anatolia in that it is continuous from late Middle

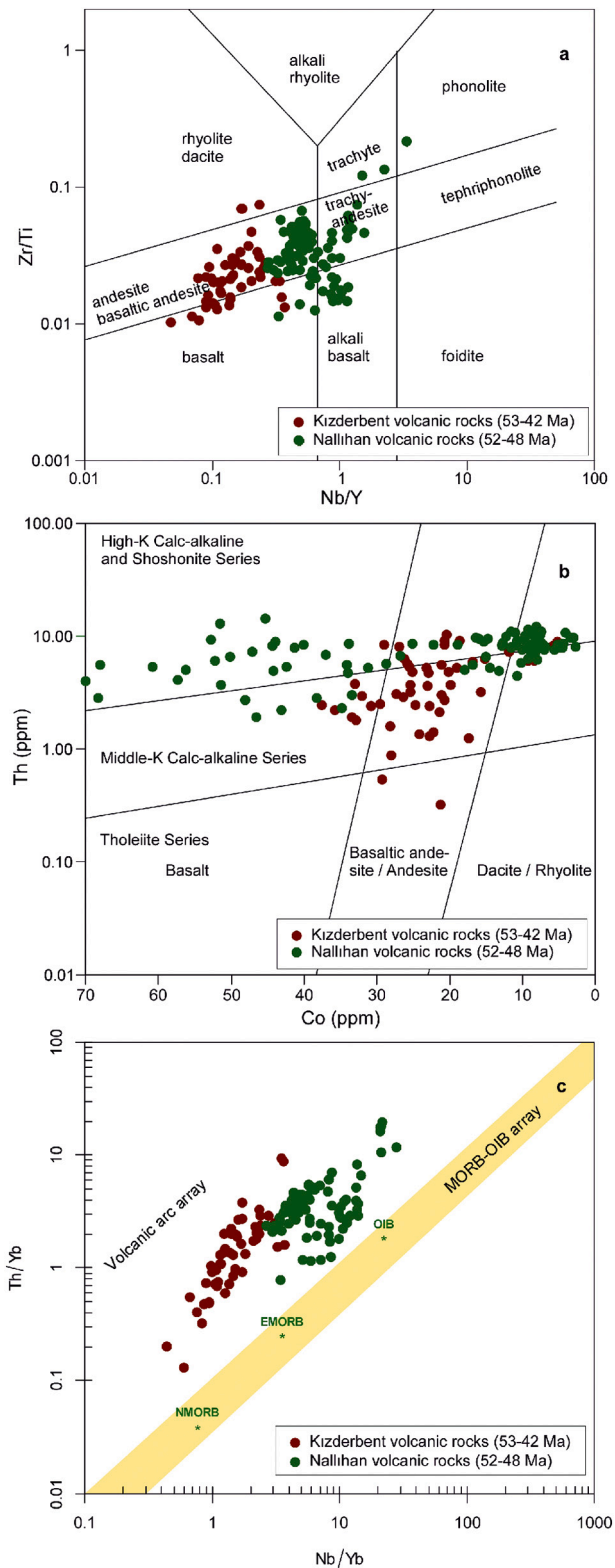


Fig. 11. a. Nb/Y vs. Zr/Ti classification diagram (Pearce, 1996) showing compositional variation of the Early to Middle Eocene volcanic rocks from NW Turkey. b. Co vs Th classification diagram (Hastie et al., 2007) showing mainly middle- to high-K nature of the Eocene volcanic rocks. c. Data plotted in the Nb/Yb vs. Th/Yb diagram (Pearce, 2008) showing their orogenic nature. Data are from Gülmez et al. (2013), Yıldız et al. (2015), Kasapoğlu et al. (2016), and Büyükkahraman (2016).

Eocene to the Early Miocene (43–18 Ma, e.g., Ersoy et al., 2017; Kuşçu et al., 2019). In this respect, it is similar to the magmatism in the Rhodopes (Fig. 1). The Biga Peninsula forms part of the Thrace Basin, where there is a thick Upper Eocene – Lower Oligocene marine clastic sequence with tuff horizons (Özcan et al., 2018).

6. Eocene thermal metamorphism

The Eocene thermal event, which was responsible for magmatism, also produced regional metamorphism, which is observed in two regions in the Tavşanlı Zone (Figs. 3 and 4). In both regions Late Cretaceous high pressure – low temperature metamorphic rocks of the Tavşanlı Zone were overprinted by an Eocene low to medium pressure - high temperature metamorphism. Southeast of Uludağ, blueschist metapelite has been transformed into andalusite micaschist with the paragenesis andalusite + cordierite + biotite + muscovite + quartz + K-feldspar + plagioclase over an area of ~10 km long and ~8 km across around the Tepeldağ pluton (Okay and Satır, 2006). Eocene metamorphism was associated with folding and development of new foliation. Pressure-temperature conditions of the Eocene metamorphism were determined as 2 ± 1 kbar and 575 ± 50 °C. Rubidium-strontium muscovite and biotite ages of a micaschist sample are 46 ± 3 Ma and 39 ± 1 Ma, respectively, similar to the 45.0 ± 0.2 Ma U-Pb zircon age from the neighboring Tepeldağ Pluton (Okay and Satır, 2006).

Southeast of Sivrihisar, blueschist-facies micaschist and marble have been overprinted by a lower pressure and higher temperature regional metamorphic event of Eocene age characterized by andalusite and sillimanite (Fig. 4, Whitney et al., 2011; Seaton et al., 2013). Ar/Ar muscovite ages in the Günyüzü metamorphic rocks in the vicinity of Sivrihisar are mostly 63–59 Ma (Seaton et al., 2013), which is close to the ages of the intrusive granites (58–55 Ma). During this study, mica Ar/Ar ages were obtained from the micaschist from west of Günyüzü to constrain the extent of the Eocene metamorphism (Fig. 4). A sample (8877) close to the Karacaören granite yielded muscovite and biotite ages of ca. 50 Ma, and ca. 26 Ma, respectively (Table 1 and S2), whereas samples farther away from the granites (10,131 and 10,139) yielded Late Cretaceous ages of 84 Ma and 109 Ma (Table 1 and S2, Fig. 4). Whitney et al. (2011) regard the blueschist facies and lower pressure metamorphism as part of a progressive geological event. However, the 20 my time gap between these two events, and the close spatial and temporal association of Eocene metamorphic and granitic rocks in the Günyüzü area indicate that the Eocene event is unrelated to the high-pressure metamorphism.

7. Exhumation of the Late Paleocene – Middle Eocene plutons

The LP-ME plutons form a belt spatially distinct from the partly coeval Eocene volcanic rocks (Figs. 1 and 3). This geometry indicates post-Middle Eocene uplift and erosion to exhume the plutons, which were emplaced at depths of about 10 km (Harris et al., 1994; Köprübaşı and Aldanmaz, 2004). To constrain the exhumation of the LP-ME plutonic belt, apatite fission-track ages (AFT) were obtained from five granite samples from the Sivrihisar-Günyüzü plutons. The AFT ages range from 42 Ma to 29 Ma and indicate Middle Eocene to Early Oligocene exhumation (Table 2, Figs. 2 and 4). A single published apatite U-Th/He age of 38 Ma from the Sivrihisar Monzonite also points to a Late Eocene exhumation (Özdamar et al., 2018). The Sivrihisar-Günyüzü and Western Tavşanlı plutons are aligned around the Eskişehir Fault, a major dextral strike-slip fault (Figs. 1 and 3), which was active during the Late Eocene and Early Oligocene (35–28 Ma, Okay et al., 2008; Topuz and Okay, 2017). The exhumation of these plutons is most likely linked to transpressive activity along the Eskişehir Fault.

Table 2

Apatite fission track age data from the Late Paleocene – Middle Eocene granites from northwest Anatolia.

Name of intrusion and sample number	No. of crystals	Spontaneous		Induced		P (χ^2)	Dosimeter		Age (Ma) $\pm 1\sigma$	Mean confined track length (μm) \pm std. err.	Standart deviation	No. of tracks measured
		ρ_s	N_s	ρ_i	N_i		ρ_d	N_d				
Kadıncık 9384	20	1.79	239	0.85	1131	11.3	1.17	5824	42.1 \pm 4.3	14.06 \pm 0.15	0.91	35
Karacaören 9413	20	1.46	247	0.99	1681	31.6	1.16	5802	29.3 \pm 2.6	13.43 \pm 0.22	1.55	51
Kaymaz 9429	20	4.79	600	2.91	3644	30.4	1.15	5792	32.6 \pm 2.3	14.02 \pm 0.29	1.39	23
Sivrihisar 9404	20	6.38	751	3.41	4036	6.2	1.16	5814	37.0 \pm 2.7	13.73 \pm 0.16	1.57	100
Topkaya 9431	20	3.15	335	1.87	1984	14.3	1.14	5780	33.3 \pm 2.9	13.98 \pm 0.16	0.99	36

8. Quantifying the crustal thickness from Late Paleocene to Late Eocene

Whole-rock Sr/Y and La/Yb ratios of basic and intermediate igneous rocks from modern magmatic arcs and young collisional belts display positive correlation with crustal thickness (e.g., Hu et al., 2017; Profeta et al., 2015). Garnet is stabilized at higher crustal pressures at the expense of plagioclase during the high-pressure fractionation of basic to felsic melts. Therefore, melts which are products of high-pressure fractionation will be depleted in garnet-compatible elements (heavy rare earth elements, Y, Sc) and enriched in plagioclase-compatible elements (e.g., Sr). Thus, melts will tend to have higher La/Yb and Sr/Y ratios when the crust is thick.

We calculated the crustal thicknesses using the empirically derived formulation for Sr/Y ratio of Hu et al. (2017). The results are given in Table S3. During the calculations, we used the bulk rock compositions with SiO₂ = 55–72 wt%, MgO = 0.5–6.0 wt%, Rb/Sr < 0.35, Sr/Y < 60 and La < 60 ppm, as suggested by Hu et al. (2017). The Rb/Sr filter is used to discard samples that were strongly influenced by fractionation within the crust. In addition, analyses with high loss on ignition values (LOI > 3 wt%) are discarded. High values of loss on ignition values pose serious problems in the Early to Middle Eocene volcanic rocks (1.53 to 9.50 wt%) (Table S3).

Sr/Y and chondrite-normalized La/Yb ratios of the Late Paleocene igneous rocks (58–54 Ma) are high, and decrease in the Early to Middle Eocene igneous rocks (54–45 Ma) and increase again in the Late Eocene igneous rocks (ca. 38 Ma), although the latter is based only on data from the South Kapıdağ pluton (Fig. 12a, b, Table S3). These values display large scatter only in composite plutons such as Orhaneli. Calculation of the crustal thickness based on the Sr/Y ratios yielded crustal thicknesses of 63–66 km for the Late Paleocene, and 35–46 km for the Early to Middle Eocene and 60–65 km during Late Eocene (38 Ma) (Fig. 12c). The calculated crustal thicknesses show a close agreement with the time periods when the Pontides subsided below sea level, and emerged above sea level, as discussed below.

9. Depositional environment during the Late Paleocene – Middle Eocene magmatic flare-up

The depositional and tectonic environments before and during the LP-ME magmatism can be deduced from the geological record of the Pontides and the Anatolide-Tauride Block. The complete subduction of the İzmir-Ankara-Erzincan oceanic lithosphere was followed by the continental subduction of the northern margin of the Anatolide-Tauride Block during the Late Cretaceous at ca. 80 Ma (Sherlock et al., 1999). This is reflected in the blueschist facies metamorphism observed in the Tavşanlı Zone. The blueschists and the overlying ophiolites are unconformably overlain by shallow marine Lower Eocene limestone and sandstone (Fig. 1, Özgen-Erdem et al., 2007). The period between the latest Cretaceous and Early Eocene (80–56 Ma) was a time of uplift and

erosion for the Tavşanlı Zone.

The Mesozoic-Cenozoic sedimentary record is more complete in the Pontides, which constituted the active margin during the Late Cretaceous. It is best preserved in the Central Sakarya Basin (Figs. 3, 1980; Ocakoğlu et al., 2018; Mueller et al., 2019). Here, Upper Cretaceous (Campanian) deep marine turbidites pass upwards into shallow marine sandstone, limestone and eventually to continental red beds of Paleocene age (Fig. 2). The transition from turbidites to continental red beds (flysch to molasse transition) is diachronic and youngs from Early Paleocene (ca. 63 Ma) in the south in the Nallıhan region (Ocakoğlu et al., 2018) to the Late Paleocene (ca. 58 Ma) in the north in the Göynük region. The diachronic uplift reflects the northward migration of deformation front following the Early Paleocene collision between the Pontides and the Anatolide-Tauride Block. Convergence between Africa and Eurasia shows a major decrease during the latest Cretaceous and Paleocene (Fig. 2, Smith, 2006) possibly reflecting the continental collision. By the Late Paleocene (56 Ma) the whole collision zone has become subareal. Early Paleocene (ca. 63 Ma) can be taken as the beginning of the continental collision, defined as the first contact of the opposing continental plates.

The Late Paleocene uplift and erosion were soon followed by a major phase of marine and continental sedimentation starting in the Early Eocene (ca. 56 Ma) and continuing into the early Middle Eocene (ca. 45 Ma, Fig. 2, Özcan et al., 2012). Volcanism accompanied the Eocene sedimentation, and Kızderbent volcanic and volcanoclastic rocks are commonly intercalated with shallow marine and continental sedimentary rocks. The thickness of the volcano-sedimentary Eocene sequence in northwest Turkey ranges up to 1500 m (Özcan et al., 2012). Northeast-southwest (N48E) extension during the Eocene is indicated by the regional dyke swarm on the Armutlu Peninsula (Fig. 10c, d). The strike of the regional dyke swarms is parallel to the σ_1 - σ_2 plane, and the normal to the dykes represent the minimum compressive principal stress σ_3 . Marine sedimentation ceased at the end of the Middle Eocene (41 Ma) with the uplift of western and central Anatolia and the whole of the Pontides except the Thrace Basin, became a land area (Okay et al., 2020a; Özcan et al., 2018). Close to the İzmir-Ankara suture, however, the shortening started already in the Early Eocene as documented in the Sarıcakaya foreland basin (Mueller et al., 2019).

The geochemistry of the LP-ME plutonic rocks indicates crustal thinning at the beginning of the Early Eocene (ca. 55 Ma, Fig. 11). The Early Eocene also corresponds to an increase in the convergence between Africa and Eurasia (Fig. 2, Smith, 2006). The increase in convergence can be related to the northward subduction of the southern Tethys. Although the İzmir-Ankara ocean closed in the Paleocene, the southern branch of the Neo-Tethys between the Anatolide-Tauride Block and Africa-Arabia stayed open until the Miocene (Okay et al., 2010). The present Eastern Mediterranean represents a relict of this ocean.

The sedimentary record indicates that the LP-ME magmatism started during the final stages of the Paleocene collision along the İzmir-Ankara-Erzincan suture and continued during the Early-Middle Eocene

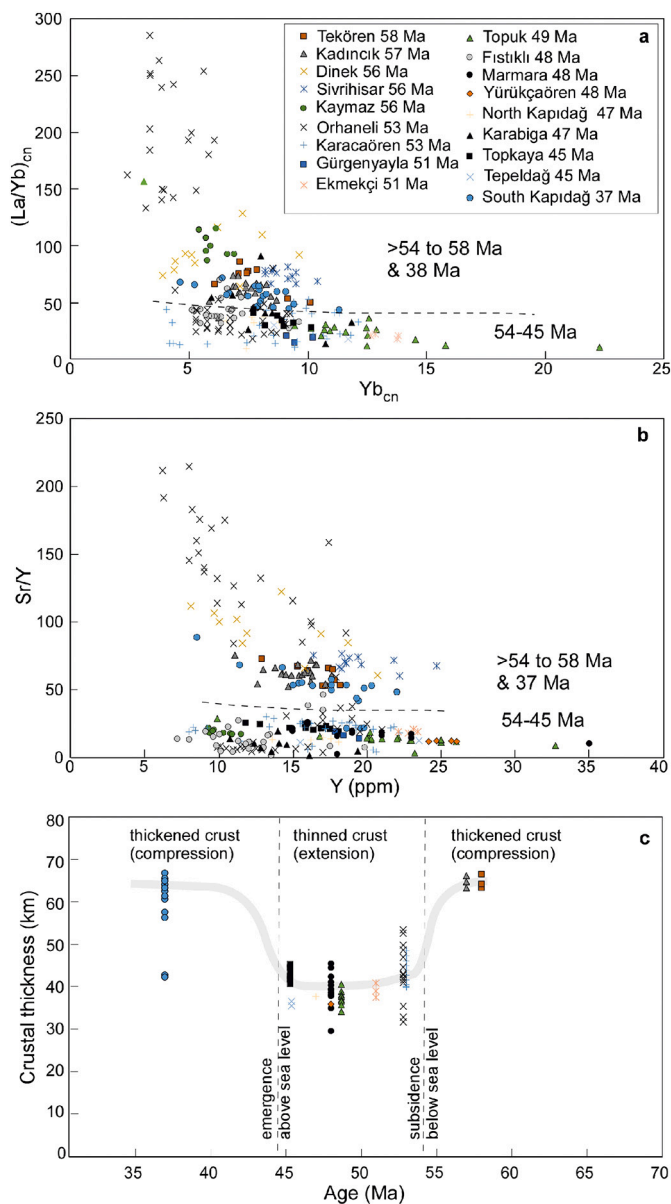


Fig. 12. a-b. Yb_{cn} vs. $(La/Yb)_{cn}$, and Y vs Sr/Y diagrams for Late Paleocene–Eocene plutonic rocks from NW Anatolia. c. Temporal variation of crustal thickness calculated from Sr/Y ratios of the intermediate plutonic rocks after Hu et al. (2017). Compositional data are from Harris et al. (1994), Köprübaşı and Aldanmaz (2004), Kibici et al. (2008), Ustaömer et al. (2009), Altunkaynak et al. (2012) Çelebi and Köprübaşı (2014), Demirbilek et al. (2018), Sunal et al. (2019), Bağcı et al. (2019), Gürarlan and Altunkaynak, (2019) and Özyurt and Altunkaynak (2020).

extension and ended with the uplift of western and central Anatolia.

10. Discussion on the origin of the Late Paleocene – Middle Eocene magmatism

Any mechanism for the origin of the LP-ME magmatism must be compatible with the following major constraints. 1) The LP-ME magmatic rocks in northwestern Turkey occur in a ca. 150–200 km wide, roughly E-W trending belt, and extend eastwards without any spatial or temporal break into the Eastern Pontides, Lesser Caucasus and Urumieh-Dokhtar belt in Iran (Fig. 1b). In this 3000 km long belt, Eocene magmatism shows similar geochemical and tectonic features. 2) The magmatism started at the Late Paleocene (58 Ma) during the late

stages of the continental collision and was most voluminous during Early to early Middle Eocene extension (53 to 45 Ma) and declined substantially after 45 Ma with the uplift of Anatolia above sea level. In the Urumieh-Dokhtar belt in Iran high-flux magmatism also took place between 53 and 37 Ma (Mokhtari et al., 2022). 3) The geochemistry of the LP-ME magmatic rocks show typical subduction zone signatures with little or no evidence for crustal and asthenospheric melting, e.g., consistent negative Nb-Ta, Ti anomalies on the multi-element variation diagrams. Rocks that represent products of pure crustal and asthenospheric melting have not been documented to date. 4) The magmatism was post-tectonic with respect to the formation of the İzmir-Ankara suture but was coeval with the northward subduction of the southern branch of the Neo-Tethys.

Slab-breakoff, lithospheric delamination and subduction were suggested as the cause of the LP-ME magmatism in northwest and central Anatolia. Most studies relate the LP-ME magmatism in northwest Anatolia to slab breakoff following the Paleocene continental collision (Altunkaynak et al., 2012; Altunkaynak and Dilek, 2013; Dokuz et al., 2019; Ersoy et al., 2017; Ersoy and Palmer, 2013; Gülmez et al., 2013; Gürarlan and Altunkaynak, 2019; Karacık et al., 2008; Kasapoğlu et al., 2016; Keskin et al., 2008). Slab breakoff is frequently used as a model to explain post-collisional magmatism (e.g., Davies and von Blanckenburg, 1995). It is a natural consequence of continental subduction; the down-going dense oceanic lithosphere will eventually separate from the attached buoyant continental lithosphere (Davies and von Blanckenburg, 1995). The hot asthenosphere rises and fills the space between the subducting continental and oceanic slabs, and generates magmatism and uplift. The main predictions of the slab breakoff model can be summarized as follows: 1) The slab breakoff occurs after the continental subduction, and is largely coeval with the continental collision (e.g., von Blanckenburg and Davies, 1995). 2) It results in the uplift of the collision zone. Modelling studies show a sharp breakoff signal in the topography over the collision zone with the uplift rate inversely related to the depth of breakoff (e.g., Duretz et al., 2011). However, in practice it is difficult to separate uplift due to continental collision from that due to slab breakoff. 3) Magmatism and uplift associated with slab breakoff occurs in a relatively narrow zone along the suture.

In slab breakoff models the LP-ME magmatism in northern Turkey is linked to the slab breakoff of the İzmir-Ankara oceanic lithosphere. The İzmir-Ankara ocean closed in the Paleocene with the collision of the Pontides and the Anatolide-Tauride Block, however, the southern branch of the Neo-Tethys, which extended into Iran, existed until the Miocene. The Eocene magmatism in the Urumieh-Dokhtar belt in Iran is generally attributed to the northeastward subduction of this southern branch of Neo-Tethys (e.g., Stern et al., 2021). It is highly unlikely that the 3000-km-long LP-ME belt magmatic belt was formed by slab breakoff in the west and by subduction in the east, especially since magmatism along the belt shows similar temporal and geochemical features. It is highly probable that there is a single cause for the LP-ME magmatic belt in Anatolia and Iran. Furthermore, recent numeric models show that the slab break cannot produce much magmatism as commonly postulated (e.g., Garzanti et al., 2018). Thus, we regard the slab breakoff model an improbable cause for the LP-ME magmatic flare-up.

Köprübaşı and Aldanmaz (2004) suggested lithospheric delamination as the cause of the Eocene magmatism. Lithospheric delamination involves the detachment of the lithospheric mantle and lowermost part of crust following crustal and lithospheric thickening. The asthenospheric mantle flows into the space created by the detached lithospheric mantle and creates uplift, extension and magmatism (e.g., Bird, 1979). A prerequisite of lithospheric delamination is major crustal thickening, which allows the dense lower lithospheric mantle to detach and sink into the asthenosphere. In northwest Anatolia crustal thickening following the Paleocene collision is confined to the Tavşanlı Zone. Paleocene sedimentary sequences are preserved in the Pontides within a few ten kilometers of the İzmir-Ankara suture (Fig. 3). In the Menderes Massif

the pre-metamorphic sedimentary sequence extends up to the Paleocene and locally into Early Eocene. The continental collision between the Pontides and the Anatolide-Tauride Block did not lead to large scale crustal thickening because part of the convergence was taken up by the subduction of the southern branch of the Neo-Tethys. Furthermore, delamination occurs in a broad semi-circular area, such as the southern Sierra Nevada in California (e.g., Saleeby et al., 2003); it is difficult to attribute the 3000 km Eocene magmatic belt to this process, especially considering that the collision along the Zagros suture was Miocene in age (e.g., Okay et al., 2010; Stern et al., 2021). Hence, delamination is an unlikely cause of the Eocene magmatism.

The third model for the LP-ME magmatism is subduction. Episodic magmatic flare-ups in arcs are a widely observed phenomenon (e.g., Ducea et al., 2015), and might be related to tapping of previously stored magma in the mantle lithosphere (e.g., Chapman et al., 2021). Tomographic studies indicate the presence of a major subducted slab under the Aegean reaching a depth of ~1400 km (e.g., Wortel and Spakman, 2000). This shows that the subduction of the southern Neo-Tethys goes back at least to the Eocene and possibly earlier. An argument against the magmatic arc origin for the LP-ME magmatism is the 450 km distance between the present Hellenic trench and the LP-ME magmatic rocks. In subduction zones the mean distance between the trench and volcanic arc is 230 ± 84 km, although it can be as large as 570 km (e.g., Heuret et al., 2011). However, the Aegean region and the Western Anatolia have undergone major north-south extension in the Neogene, and the distance was smaller during the Eocene. Most subduction zones are characterized by the presence of a magmatic arc, fore-arc basin and subduction-accretion complex. During the LP-ME (58–45 Ma) magmatism, the region between the arc and the trench in western Anatolia was, on the other hand, mostly an erosional area. Arguments in favor of the subduction model include: a) The Eocene magmatic belt extends for over 3000 km from northwest Turkey to Iran (Fig. 1b); such a long magmatic belt is difficult to generate except above a subduction zone. b) The geochemistry of the LP-ME Paleocene-Eocene magmatic rocks are similar to those formed above subduction zones. c) The southern branch of the Neo-Tethys was subducting northward during the Eocene.

11. Conclusions

The main conclusions of this study are as follows:

1. Late Paleocene –Middle Eocene represents a period of intense magmatism in the Pontides extending into the Lesser Caucasus and Iran forming a belt of over 3000 km in length (Fig. 1b).
2. New U-Pb zircon data indicate that the magmatism in northwest Anatolia started in the Late Paleocene (58 Ma) during the final stages of continental collision. It was particularly intense during the Early to early Middle Eocene (53–45 Ma) extension and decreased abruptly at 45 Ma with the uplift of Anatolia (Fig. 2).
3. The LP-ME plutonic belt, ca. 410 km long and ca. 40 km wide, cuts across the Izmir-Ankara-Erzincan suture (Fig. 3). New apatite fission tract ages indicate that the plutonic belt was exhumed during Late Eocene-Early Oligocene (44–28 Ma, Fig. 2), possibly by transpression along the dextral strike-slip Eskişehir Fault.
4. Crustal thickness variations based on whole rock Sr/Y ratios of the intermediate igneous rocks point to the presence of a thickened crust during Late Paleocene to earliest Ypresian (58–54 Ma), and of a relatively thinned crust during middle Ypresian to middle Lutetian (52–45 Ma), and relatively thickened crust during Late Eocene-Early Oligocene (38–28 Ma, Fig. 12). These periods are compatible with the depositional environments in the Pontides. The most voluminous magmatism occurred during the period of relatively thinned crust at 53–47 Ma when the NW Anatolia was below sea level (ca. 53–45 Ma).
5. All of the LP-ME magmatic rocks show subduction-related geochemical signatures. The volcanic rocks were derived mainly

from juvenile melts, and the intrusions from the juvenile melts that assimilated variable amounts of crustal material. So far, there are no documented rock types that could be interpreted as products of pure crustal or asthenospheric melts.

6. The LP-ME magmatic flare-up probably occurred in a magmatic arc above the northward subducting southern Neo-Tethys ocean.

Supplementary data to this article can be found online at <https://doi.org/10.1016/j.lithos.2022.106816>.

Declaration of Competing Interest

The authors declare that they have no known competing financial interests or personal relationships that could have appeared to influence the work reported in this paper.

Acknowledgments

This study is supported by the TÜBİTAK projects 113R007 and 116Y127 and by TÜBA. We thank Gürsel Sunal and Ezgi Sağlam for help with zircon data analysis and Ersin Koralay for one of the samples. Roberts Moritz and an anonymous reviewer provided detailed and constructive comments, which improved the manuscript.

References

- Akkiraz, M.S., Nazik, A., Özgen-Erdem, N., Durak, S.D., 2022. First micropalaeontological record from the early and Middle Eocene Mamuca Formation of the Dümrek Basin, western Central Anatolia, Turkey: Biostratigraphy, depositional history and palaeoclimate. *J. Asian Earth Sci.* 224, 105036.
- Altunkaynak, Ş., Dilek, Y., 2013. Eocene mafic volcanism in northern Anatolia: its causes and mantle sources in the absence of active subduction. *Inter. Geol. Rev.* 55, 1641–1659.
- Altunkaynak, Ş., Sunal, G., Aldanmaz, E., Genç, C.Ş., Dilek, Y., Furnes, H., Folland, K., Yang, J., Yıldız, M., 2012. Eocene Granitic Magmatism in NW Anatolia (Turkey) revisited: New implications from comparative zircon SHRIMP U–Pb and 40Ar–39Ar geochronology and isotope geochemistry on magma genesis and emplacement. *Lithos* 155, 289–309.
- Arslan, M., Temizel, I., Abdioglu, E., Kolayli, H., Yücel, C., Boztuğ, D., Şen, C., 2013. ⁴⁰Ar–³⁹Ar dating, whole-rock and Sr–Nd–Pb isotope geochemistry of post-collisional Eocene volcanic rocks in the southern part of the Eastern Pontides (NE Turkey): implications for magma evolution in extension-induced origin. *Contrib. Mineral. Petrol.* 166, 113–142.
- Bağcı, M., Demirbilek, M., İlbeyli, N., Yıldız, A., Kibici, Y., 2019. Geochronological and geochemical constraints and origin of the Tavşanlı Zone plutonic rocks (NW Turkey). *Turk. J. Earth Sci.* 28, 60–84.
- Bird, P., 1979. Continental delamination and the Colorado Plateau. *J. Geophys. Res.* 84, 7561–7571.
- Büyükkahraman, G., 2016. Petrology of Eocene volcanic rocks from the Central Sakarya Zone (northwestern Anatolia, Turkey): new evidence from Ar–Ar and Sr–Nd isotope determinations. *Arab. J. Geosci.* 9, 675.
- Çelebi, D., Köprübaşı, N., 2014. The geochemical and Sr–Nd isotopic characteristics of Eocene to Miocene NW Anatolian granitoids: Implications for magma evolution in a post-collisional setting. *J. Asian Earth Sci.* 93, 275–287.
- Chapman, J.B., Shields, J.E., Ducea, M.N., Paterson, S.R., Attia, S., Ardill, K.E., 2021. The causes of continental arc flare ups and drivers of episodic magmatic activity in Cordilleran orogenic systems. *Lithos* 398–399, 106307.
- Davies, J.H., von Blanckenburg, F., 1995. Slab breakoff: a model of lithosphere detachment and its test in the magmatism and deformation of collisional orogens. *Earth Planet. Sci. Letters* 129, 85–102.
- Delaloye, M., Bingöl, E., 2000. Granitoids from western and northwestern Anatolia: geochemistry and modelling of geodynamic evolution. *Int. Geol. Rev.* 42, 241–268.
- Demirbilek, M., Mutlu, H., Fallick, A.E., Sariz, K., Kibici, Y., 2018. Petrogenetic evolution of the Eocene granitoids in eastern part of the Tavşanlı Zone in northwestern Anatolia, Turkey. *Lithos* 314–315, 236–259.
- Dokuz, A., Aydın, F., Karli, O., 2019. Postcollisional transition from subduction- to intraplate-type magmatism in the eastern Sakarya zone, Turkey: Indicators of northern Neotethyan slab breakoff. *Geol. Soc. Am. Bull.* 131, 1623–1642.
- Ducea, M.N., Paterson, S.R., DeCelles, P.G., 2015. High-volume magmatic events in subduction systems. *Elements* 11, 99–104.
- Duret, T., Gerya, T.V., May, D.A., 2011. Numerical modelling of spontaneous slab breakoff and subsequent topographic response. *Tectonophysics* 502, 244–256.
- Ersoy, E.Y., Palmer, M.R., 2013. Eocene-Quaternary magmatic activity in the Aegean: Implications for mantle metasomatism and magma genesis in an evolving orogeny. *Lithos* 180–181, 5–24.
- Ersoy, E.Y., Akal, C., Genç, Ş.C., Candan, O., Palmer, M.R., Prelević, D., Uysal, İ., Mertz-Kraus, R., 2017. U–Pb zircon geochronology of the Paleogene-Neogene volcanism in

- the NW Anatolia: its implications for the late Mesozoic-Cenozoic geodynamic evolution of the Aegean. *Tectonophysics* 717, 284–301.
- Frost, B.R., Barnes, C.G., Collins, W.J., Arculus, R.J., Ellis, D.J., Frost, C.D., 2001. A geochemical classification for granitic rocks. *J. Petrol.* 42, 2033–2048.
- Gallhofer, D., von Quadt, A., Peytcheva, I., Schmid, S.M., Heinrich, C.A., 2015. Tectonic, magmatic, and metallogenic evolution of the Late Cretaceous arc in the Carpathian-Balkan orogen. *Tectonics* 34, 1813–1836.
- Garzanti, E., Radeff, G., Malusà, M.G., 2018. Slab breakoff: a critical appraisal of a geological theory as applied in space and time. *Earth Sci. Rev.* 177, 303–319.
- Grosjean, M., Moritz, R., Rezeau, H., Hovakimyan, S., Ulianov, A., Chiaradia, M., Melkonyan, R., 2022. Arabia-Eurasia convergence and collision control on Cenozoic juvenile K-rich magmatism in the South Armenian block. *Earth-Science Reviews* 226, 103949. <https://doi.org/10.1016/j.earscirev.2022.103949>.
- Gülmez, F., Genç, S.C., Keskin, M., Tüysüz, O., 2013. A post-collision slab-breakoff model for the origin of the Middle Eocene magmatic rocks of the Armutlu-Almacik belt, NW Turkey and its regional implications. *Geol. Soc. Lond.* 372, 107–139.
- Güraslan, I.N., Altunkaynak, Ş., 2019. Role of mantle and lower continental crust in the genesis of Eocene postcollisional granitoids: Insights from the Topuk pluton (NW Turkey). *J. Asian Earth Sci.* 179, 365–384.
- Harris, N.B.W., Kelley, S., Okay, A.I., 1994. Post-collision magmatism and tectonics in northwest Anatolia. *Contrib. Mineral. Petrol.* 117, 241–252.
- Hastie, A.R., Kerr, A.C., Pearce, J.A., Mitchell, S.F., 2007. Classification of altered volcanic island arc rocks using immobile trace elements: development of the Th–Co discrimination diagram. *J. Petrol.* 48, 2341–2357.
- Heuret, A., Lallemand, S., Funicello, F., Piromallo, C., Faccenna, C., 2011. Physical characteristics of subduction interface type seismogenic zones revisited. *Geochem. Geophys. Geosyst.* 12, Q01004. <https://doi.org/10.1029/2010GC003230>.
- Hu, F., Ducea, M.N., Liu, S., Chapman, J.B., 2017. Quantifying crustal thickness in continental collisional belts: Global perspective and a geologic application. *Sci. Rep.* 7, 1–10.
- Irvine, T.N., Baragar, W.R.A., 1971. A guide to the chemical classification of the common volcanic rocks. *Can. J. Earth Sci.* 8, 523–548.
- Karakç, Z., Yılmaz, Y., Pearce, J.A., Ece, Ö.I., 2008. Petrochemistry of the south Marmara granitoids, northwest Anatolia. *Turkey. Int. J. Earth Sci.* 97, 1181–1200.
- Kasapoğlu, B., Ersoy, E.Y., Uysal, İ., Palmer, M.R., Zack, T., Koray, E.O., Karlsson, A., 2016. The petrology of Paleogene volcanism in the Central Sakarya, Nallihan Region: Implications for the initiation and evolution of post-collisional, slab break-off-related magmatic activity. *Lithos* 246–247, 81–98.
- Kaygusuz, A., Yücel, C., Arslan, M., Temizel, İ., Yi, K., Jeong, Y.-J., Siebel, W., Sipahi, F., 2020. Eocene I-type magmatism in the Eastern Pontides, NE Turkey: insights into magma genesis and magma-tectonic evolution from whole-rock geochemistry, geochronology and isotope systematics. *Int. Geol. Rev.* 162, 1406–1432.
- Keskin, M., Genç, Ş.C., Tüysüz, O., 2008. Petrology and geochemistry of post-collisional Middle Eocene volcanic units in North-Central Turkey: Evidence for magma generation by slab breakoff following the closure of the Northern Neotethys Ocean. *Lithos* 104, 267–305.
- Kıbıcı, Y., İlbeyli, N., Yıldız, A., Bağcı, M., 2008. Geochemical constraints on the genesis of the Günyüzü pluton, Northwest Anatolia, Turkey. *Int. Geol. Rev.* 50, 931–947.
- Köprübaşı, N., Aldanmaz, E., 2004. Geochemical constraints on the petrogenesis of Cenozoic I-type granitoids in Northwest Anatolia, Turkey: evidence for magma generation by lithospheric delamination in a post-collisional setting. *Int. Geol. Rev.* 46, 705–729.
- Kürkçüoğlu, B., Furman, T., Hanan, B., 2008. Geochemistry of post-collisional mafic lavas from the North Anatolian Fault Zone, Northwestern Turkey. *Lithos* 101, 416–434.
- Kuşcu, İ., Tosdal, R.M., Gençlioğlu-Kuşcu, G., 2019. Episodic porphyry Cu (–Mo–Au) formation and associated magmatic evolution in Turkish Tethyan collage. *Ore Geol. Rev.* 107, 119–154.
- Marchev, P., Georgiev, S., Raicheva, R., Peytcheva, I., Quadt, A., Ovtcharova, M., Bonev, N., 2013. Adakitic magmatism in post-collisional setting: An example from the Early–Middle Eocene Magmatic Belt in Southern Bulgaria and Northern Greece. *Lithos* 180–181, 159–180.
- Middlemost, E.A.K., 1994. Naming materials in the magma/igneous rock system. *Earth Sci. Rev.* 37, 215–244.
- Mokhtari, M.A.A., Kouhestani, H., Pang, K.-N., Hsu, S.-C., Chung, S.-L., Lee, H.Y., 2022. Early Eocene high-Sr/Y magmas from the Urumieh-Dokhtar paleo-arc, Iran: Implications for the origin of high-flux events in magmatic arcs. *Lithos* 416–417, 106656.
- Moritz, R., Popkhadze, N., Hässig, M., Golay, T., Lavoie, J., Gugushvili, V., Ulianov, A., Ovtcharova, M., Grosjean, M., Chiaradia, M., Dumitrica, M., 2020. At the crossroads of the Lesser Caucasus and the Eastern Pontides: late Cretaceous to early Eocene magmatic and geodynamic evolution of the Bolnisi district, Georgia. *Lithos* 378–379, 105872.
- Mueller, M.A., Licht, A., Campbell, C., Ocañoğlu, F., Taylor, M.H., Burch, L., Ugrai, T., Kaya, M., Kurtoglu, B., Coster, P.M.C., Métais, G., Beard, K.C., 2019. Collision chronology along the İzmir-Ankara-Erzincan suture zone: Insights from the Sarıcakaya Basin, western Anatolia. *Tectonics* 38, 3652–3674.
- Nouri, F., Azizi, H., Asahara, Y., Stern, R.J., 2021. A new perspective on Cenozoic calc-alkaline and shoshonitic volcanic rocks, eastern Saveh (central Iran). *Int. Geol. Rev.* 63, 476–503.
- Ocañoğlu, F., Hakyemez, A., Açıkalın, S., Özkan Altuner, S., Büyükmeriç, Y., Licht, A., Demircan, H., Şafak, Ü., Yıldız, A., Ömer Yılmaz, I., Wagreich, M., Campbell, C., 2018. Chronology of subduction and collision along the İzmir-Ankara suture in Western Anatolia: records from the Central Sakarya Basin. *Int. Geol. Rev.* 61, 1244–1269.
- Okay, A.I., Satır, M., 2006. Geochronology of Eocene plutonism and metamorphism in northwest Turkey: evidence for a possible magmatic arc. *Geodin. Acta* 19, 251–266.
- Okay, A.I., Satır, M., Zattin, M., Cavazza, W., Topuz, G., 2008. An Oligocene ductile strike-slip shear zone: Uludağ Massif, northwest Turkey – implications for the escape tectonics. *Geol. Soc. Am. Bull.* 120, 893–911.
- Okay, A.I., Zattin, M., Cavazza, W., 2010. Apatite fission-track data for Miocene Arabia-Eurasia collision. *Geology* 38, 35–38.
- Okay, A.I., Zattin, M., Özcan, E., Sunal, G., 2020a. Uplift of Anatolia. *Turk. J. Earth Sci.* 29, 696–713.
- Okay, A.I., Sunal, G., Sherlock, S., Kylander-Clark, A.R.C., Özcan, E., 2020b. İzmir-Ankara suture as a Triassic to Cretaceous plate boundary—Data from Central Anatolia. *Tectonics* 38 (e2019TC005849).
- Özcan, Z., Okay, A.I., Özcan, E., Hakyemez, A., Özkan-Altiner, S., 2012. Late Cretaceous–Eocene geological evolution of the Pontides in Northwest Turkey between the Black Sea coast and Bursa. *Turk. J. Earth Sci.* 21, 933–960.
- Özcan, E., Okay, A.I., Bürkan, K.A., Yücel, A.O., Özcan, Z., 2018. The Bartonian–Priabonian marine record of the Biga Peninsula, NW Anatolia (Turkey): larger benthic foraminifera, revised stratigraphy and implications for the regional geology. *Geol. Acta* 16, 163–187.
- Özdamar, Ş., Sunal, G., Demiroğlu, M., Yaltrak, C., Billor, Z., Georgiev, S., Hames, W., Dunkl, I., Aydın, H., 2018. Metamorphism, magmatism and exhumation history of the Tavşanlı Zone, NW Turkey: new petrological constraints. *Turk. J. Earth Sci.* 27, 269–293.
- Özgen-Erdem, N., Akyaz, M., Karabaşoğlu, A., 2007. Biostratigraphic interpretation and systematics of Alveolina assemblages from the Ilerdian–Cuisian limestones of Southern Eskişehir. *Central Turkey. J. Asian Earth Sci.* 29, 911–927.
- Özyurt, M., Altunkaynak, Ş., 2020. Origin of Eocene adakitic magmatism in northwest Turkey. *J. Asian Earth Sci.* 190, 104–147.
- Pearce, J.A., 1996. A user's guide to basalt discrimination diagrams. In: Wyman, D.A. (Ed.), *Trace Element Geochemistry of Volcanic Rocks: Applications for Massive Sulphide Exploration*. Geological Association of Canada, Short Course Notes, vol. 12, pp. 79–113.
- Pearce, J.A., 2008. Geochemical fingerprinting of oceanic basalts with applications to ophiolite classification and the search for Archean oceanic crust. *Lithos* 100, 14–48.
- Peccerillo, A., Taylor, S.R., 1976. Geochemistry of Eocene calc-alkaline volcanic rocks from the Kastamonu area, Northern Turkey. *Contrib. Mineral. Petrol.* 58, 63–81.
- Perkins, R., Cooper, F.J., Condon, D.J., Tattitch, B., Naden, J., 2018. Post-collisional Cenozoic extension in the northern Aegean: The high-K to shoshonitic intrusive rocks of the Maronia Magmatic Corridor, northeastern Greece. *Lithosphere* 10, 582–601.
- Plunder, A., Agard, P., Chopin, C., Pourteau, A., Okay, A.I., 2015. Accretion, underplating and exhumation along a subduction interface: From subduction initiation to continental subduction (Tavşanlı zone, W. Turkey). *Lithos* 226, 233–254.
- Profeta, L., Ducea, M.N., Chapman, J.B., Paterson, S.R., Gonzales, S.M.H., Kirsch, M., Petrescu, L., DeCelles, P.G., 2015. Quantifying crustal thickness over time in magmatic arcs. *Sci. Reports* 5, 1–7.
- Rabayrol, F., Hart, C.J., Friedman, R.M., Spikings, R.A., 2021. Diachronous magmatic and Cu–Au–Mo metallogenic responses to slab roll-back initiation from Northwest Anatolia to the Balkans, Western Tethyan Eocene magmatic belt. *Society of Economic Geologists* 17–28. Sp. Publ., no. 24.
- Robertson, A.H.F., Parlak, O., Ustaömer, T., 2013. Late Palaeozoic–Early Cenozoic tectonic development of Southern Turkey and the easternmost Mediterranean: evidence from the inter-relations of continental and oceanic units. In: Robertson, A.H.F., Parlak, O., Ünlügenç, U.C. (Eds.), *Geological development of the Anatolian Continent and the Easternmost Mediterranean Region*. *Geol. Soc. London. Sp. Publ.* 372, 9–48. <https://doi.org/10.1144/SP372.22>.
- Şahin, M., Yaltrak, C., Karakç, Z., 2019. A case study of compression to escape Tectonic transition: tectonic evolution of the Nallihan Wedge and comparison with the Tercan Wedge (Eastern Mediterranean, Turkey). *J. Asian Earth Sci.* 174, 311–331.
- Saleeby, J., Ducea, M., Clemens-Knott, D., 2003. Production and loss of high-density batholithic root, southern Sierra Nevada. *California. Tectonics* 22, 1064.
- Schleiffarth, W.K., Darin, M.H., Reid, M.R., Umhoefer, P.J., 2018. Dynamics of episodic Late Cretaceous–Cenozoic magmatism across Central to Eastern Anatolia: New insights from an extensive geochronology compilation. *Geosphere* 14, 1990–2008. <https://doi.org/10.1130/GES01647.1>.
- Seaton, N.C.A., Teyssier, C., Whitney, D.L., Heizler, M.T., 2013. Quartz and calcite microfabric transitions in a pressure and temperature gradient, Sivrihisar. *Turkey. Geodin. Acta* 26, 191–206.
- Şen, F., 2020. Middle Eocene high-K acidic volcanism in the Princes' Islands (İstanbul) and its geodynamic implications. *Turk. J. Earth Sci.* 29, 208–219.
- Sherlock, S., Kelley, S.P., Inger, S., Harris, N., Okay, A.I., 1999. ⁴⁰Ar–³⁹Ar and Rb–Sr geochronology of high-pressure metamorphism and exhumation history of the Tavşanlı Zone, NW Turkey. *Contrib. Mineral. Petrol.* 137, 46–58.
- Shin, T.A., Catlos, E.J., Jacob, L., Black, K., 2013. Relationships between very high pressure subduction complex assemblages and intrusive granitoids in the Tavşanlı Zone, Sivrihisar Massif, central Anatolia. *Tectonophysics* 595–596, 183–197.
- Smith, A.G., 2006. Tethyan ophiolite emplacement, Africa to Europe motions, and Atlantic spreading. In: Robertson, A.H.F., Mountrakis, D. (Eds.), *Tectonic Development of the Eastern Mediterranean Region*. *Geol. Soc., London, Sp. Publ.* 260, pp. 11–34.
- Stern, R.J., Moghadam, H.S., Pirouz, M., Mooney, W., 2021. The Geodynamic Evolution of Iran. *Annu. Rev. Earth Planet. Sci.* 49, 9–36.
- Sun, S.S., McDonough, W.F., 1989. Chemical and isotopic systematics of oceanic basalts: implications for mantle composition and processes. *Geol. Soc., London. Sp. Publ.* 42, 313–345.

- Sunal, G., Erturaç, M.K., Topuz, G., Okay, A.I., Zack, T., 2019. The Early Eocene Ekmekçi Granodiorite porphyry in the Karacabey region (western Sakarya Zone), NW Turkey. *Turk. J. Earth Sci.* 28, 589–602.
- Topuz, G., Okay, A.I., 2017. Late Eocene - Early Oligocene two-mica granites in NW Turkey (the Uludağ Massif): Water-fluxed melting products of a mafic metagraywacke. *Lithos* 268–271, 334–350.
- Topuz, G., Okay, A.I., Altherr, R., Schwarz, W.H., Siebel, W., Zack, T., Satır, M., Şen, C., 2011. Post-collisional adakite-like magmatism in the Agvanis Massif and implications for the evolution of the Eocene magmatism in the Eastern Pontides (NE Turkey). *Lithos* 125, 131–150.
- Türkoğlu, E., Zulauf, G., Linckens, J., Ustaömer, T., 2016. Dextral strike-slip along the Kapıdağ shear zone (NW Turkey): evidence for Eocene westward translation of the Anatolian plate. *Int. J. Earth Sci.* 105, 2061–2073.
- Ustaömer, P.A., Ustaömer, T., Collins, A.S., Reischpeitsch, J., 2009. Lutetian arc-type magmatism along the southern Eurasian margin: New U-Pb LA-ICPMS and whole-rock geochemical data from Marmara Island, NW Turkey. *Miner. Petrol.* 96, 177–196.
- von Blanckenburg, F., Davies, J.H., 1995. Slab breakoff: a model for syncollisional magmatism and tectonics in the Alps. *Tectonics* 14, 120–131.
- Whitney, D.L., Teyssier, C., Toraman, E., Seaton, N.C.A., Fayon, A.K., 2011. Metamorphic evolution of a structurally continuous blueschist-to-Barrovian terrane, Sivrihisar Massif, Turkey. *J. Metamorphic Geol.* 29, 193–212.
- Wortel, M.J.R., Spakman, W., 2000. Subduction and slab detachment in the Mediterranean–Carpathian region. *Science* 290, 1910–1917.
- Yıldız, A., Kibici, Y., Bağcı, M., Duşlupınar, İ., Kocabaş, C., Aritan, A.E., 2015. Petrogenesis of the post-collisional Eocene volcanic rocks from the Central Sakarya Zone (Northwestern Anatolia, Turkey): Implications for source characteristics, magma evolution, and tectonic setting. *Arab. J. Geosci.* 8, 11239–11260.